TechBriefs

National Aeronautics and Space Administration

Electronic Components and Circuits

Electronic Systems

Physical Sciences

Materials

Computer Programs

Mechanics

Machinery

Fabrication Technology

Mathematics and Information Sciences

Life Sciences

01-09 September 2001

INTRODUCTION

Tech Briefs are short announcements of innovations originating from research and development activities of the National Aeronautics and Space Administration. They emphasize information considered likely to be transferable across industrial, regional, or disciplinary lines and are issued to encourage commercial application.

Availability of NASA Tech Briefs and TSPs

Requests for individual Tech Briefs or for Technical Support Packages (TSPs) announced herein should be addressed to

National Technology Transfer Center
Telephone No. **(800) 678-6882** or via World Wide Web at **www2.nttc.edu/leads/**

Please reference the control numbers appearing at the end of each Tech Brief. Information on NASA's Commercial Technology Team, its documents, and services is also available at the same facility or on the World Wide Web at **www.nctn.hq.nasa.gov**.

Commercial Technology Offices and Patent Counsels are located at NASA field centers to provide technology-transfer access to industrial users. Inquiries can be made by contacting NASA field centers and program offices listed below.

NASA Field Centers and Program Offices

Ames Research Center
Carolina Blake
(650) 604-1754 or
cblake@mail.arc.nasa.gov

Dryden Flight Research Center
Jenny Baer-Riedhart
(661) 276-3689 or
jenny.baer-riedhart@dfrc.nasa.gov

Goddard Space Flight Center
George Alcorn
(301) 286-5810 or
galcorn@gsfc.nasa.gov

Jet Propulsion Laboratory
Merle McKenzie
(818) 354-2577 or
merle.mckenzie@jpl.nasa.gov

Johnson Space Center
Hank Davis
(281) 483-0474 or
henry.l.davis1@jsc.nasa.gov

John F. Kennedy Space Center
Jim Aliberti
(321) 867-6224 or
Jim.Aliberti-1@ksc.nasa.gov

Langley Research Center
Sam Morello
(757) 864-6005 or
s.a.morello@larc.nasa.gov

Glenn Research Center
Larry Viterna
(216) 433-3484 or
cto@grc.nasa.gov

George C. Marshall Space Flight Center
Vernotto C. McMillan
(256) 544-2615 or
vernotto.mcmillan@msfc.nasa.gov

John C. Stennis Space Center
Kirk Sharp
(228) 688-1929 or
technology@ssc.nasa.gov

NASA Program Offices
At NASA Headquarters there are seven major program offices that develop and oversee technology projects of potential interest to industry.

Carl Ray
Small Business Innovation Research Program (SBIR) & Small Business Technology Transfer Program (STTR)
(202) 358-4652 or
cray@mail.hq.nasa.gov

Dr. Robert Norwood
Office of Commercial Technology (Code RW)
(202) 358-2320 or
rnorwood@mail.hq.nasa.gov

John Mankins
Office of Space Flight (Code MP)
(202) 358-4659 or
jmankins@mail.hq.nasa.gov

Terry Hertz
Office of Aero-Space Technology (Code RS)
(202) 358-4636 or
thertz@mail.hq.nasa.gov

Glen Mucklow
Office of Space Sciences (Code SM)
(202) 358-2235 or
gmucklow@mail.hq.nasa.gov

Roger Crouch
Office of Microgravity Science Applications (Code U)
(202) 358-0689 or
rcrouch@hq.nasa.gov

Granville Paules
Office of Mission to Planet Earth (Code Y)
(202) 358-0706 or
gpaules@mtpe.hq.nasa.gov

TechBriefs

September 2001
01-09

National Aeronautics and
Space Administration

Electronic Components and Circuits

Hardware, Techniques, and Processes

Books and Reports

6 BLANK PAGE

Improved Field-Emission Cathodes

Arrays of microscopic cathodes would resist poisoning and sputtering.

NASA's Jet Propulsion Laboratory, Pasadena, California

Microscopic cathodes based on field emission (in contradistinction to thermionic emission) are undergoing development with a view toward using them as miniature or scalable sources of electrons in diverse applications that could include spacecraft thrusters, semiconductor-fabrication equipment, flat-panel display devices, miniature x-ray sources, and electrodynamic tethers and mass spectrometers. Increasing current levels can be accomplished by increasing the number of tips in an array. The basic concepts of utilizing field-emission cathodes for such applications and of scaling up by enlarging arrays are not new; the novel aspect of the present developmental cold cathodes lies in a microfabricated cathode lens and ion repeller (CLAIR) similar to an Einzel lens which will enable the integration of field-emission cathodes with electric propulsion systems, electrodynamic tethers, and instruments while meeting performance and lifetime requirements.

The performance requirements include emitter currents in the milliampere range at gate-electrode potentials between 10 and 70 V, high efficiency, and ability of emitter tips to strongly resist sputtering by impinging ions. More specifically:

- Gate potentials are required to be low in order to minimize the kinetic energies of ions bombarding emitter tips.
- In some applications, electron energies >20 eV are required to increase the space-charge current limit in plasma environments.

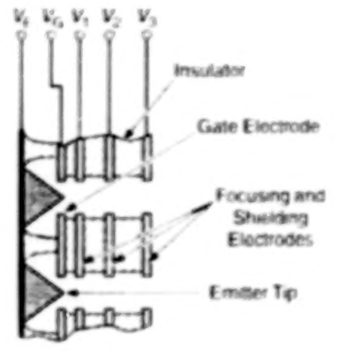

Potential, Volts				
V_E	V_G	V_1	V_2	V_3
-40	10	-10	100	-20

Dimensions, μm					
$d_{G,1}$	$d_{1,2}$	$d_{2,3}$	t_1 & t_3	t_2	ø
0.4	0.8	0.8	0.1	0.3	1.2

Side-by-Side Field-Emission Cathodes would be configured and operated to independently control electron energy and electron current density.

- For efficiency, leakage currents through gate electrodes must be kept to small fractions of emitted currents; it should not be difficult to satisfy this requirement in that gate leakage current is typically as little as a thousandth of the emitted current.
- The ability of an emitter tip to resist sputtering and poisoning with oxygen depends largely on the emitter material. It is desirable to choose an emitter material which is stable in an oxygen-rich environment, is not easily sputtered away when bombarded with ions, and has a low work function. Several materials are under investigation to meet these demands.

The figure depicts (not to scale) the configuration of an array of field-emission cathodes with CLAIR. Typical electrode thicknesses (t_i), interelectrode distances (d_i), aperture diameter (ø), and operating potentials (V_i) are shown according to one of the design concepts. Acting in concert, the V_1, V_2, and V_3 electrodes would accelerate or decelerate and focus the emitted electron beam. Singly-charged ions entering the cathode with kinetic energies below 65 eV would be retarded by the electric field between V_2 and V_3. In the case of a spacecraft thruster, the V_3 electrode would also shield the ion retarding electrodes from electrons in the thruster discharge. The CLAIR configuration without the field-emission tips can be used as an ion energy analyzer in plasma environments.

This work was done by Colleen Marrese of Caltech for **NASA's Jet Propulsion Laboratory**. *Further information is contained in a TSP [see page 1].*
NPO-21043

Si Microsensor Baseplates With Low Parasitic Capacitances

An improved design also reduces thermal-expansion mismatches.

NASA's Jet Propulsion Laboratory, Pasadena, California

An improved design for baseplates in silicon microsensors reduces parasitic capacitances between adjacent coplanar electrodes. It also reduces thermal-expansion mismatches, which are present in baseplates of older design.

Heretofore, baseplates of silicon microsensors have been made from quartz or ceramic because of concern over parasitic capacitance, which can adversely affect sensor performance. The disadvantage of using quartz or ceramic is that the coefficients of thermal expansion of these materials differ from that of silicon. The thermal-expansion mismatch subjects the sensors to undesired stresses that vary with temperature.

This **Micromachined Silicon Structure** is typical of baseplates in silicon microsensors according to the improved design. The thick dielectric layer and the p⁺ silicon epilayer are essential elements of the design to reduce the capacitance between the electrodes.

According to the improved design, the baseplate of a silicon microsensor is made from silicon, eliminating the thermal-expansion mismatch. The silicon baseplate (see figure) includes a silicon substrate, a heavily p-doped epilayer, and a thick dielectric layer made of silicon dioxide or silicon nitride

Metal electrodes are deposited on the outer surface of the dielectric layer.

The p+ epilayer serves as an electrically conductive ground plane, which contributes to reduction of the capacitance between the electrodes. The dielectric layer electrically insulates the electrodes from the ground plane. The thickness of the dielectric layer is an important element of the design. The dielectric layer must be as thick as possible, consistently with other design considerations, in order to minimize the capacitance between the electrodes and the ground plane.

This work was done by Roman Gutierrez and Tony K. Tang of Caltech for **NASA's Jet Propulsion Laboratory**. *Further information is contained in a TSP [see page 1].*

In accordance with Public Law 96-517, the contractor has elected to retain title to this invention. Inquiries concerning rights for its commercial use should be addressed to

Intellectual Property group
JPL
Mail Stop 202-233
4800 Oak Grove Drive
Pasadena, CA 91109
(818) 354-2240

Refer to NPO-20689, volume and number of this NASA Tech Briefs issue, and the page number.

Improvements in a Fast Transient-Voltage Recorder

The instrument is now more readily adjustable and reconfigurable.

John F. Kennedy Space Center, Florida

Some improvements have been made in an instrument designed expressly for recording lightning-induced transient voltages on power and signal cables. The instrument as it existed prior to the improvements was described in "Fast Transient-Voltage Recorder" (KSC-11991), *NASA Tech Briefs*, Vol. 23, No. 10 (October 1999), page 6a.

The prior version of the instrument could sample transient voltages in four channels at a rate of 20 megasamples per second (MS/s). In the improved version, the rate can be easily increased to 100 MS/s. The prior version of the instrument could handle a peak input potential of 50 V, or more if an attenuator was used. The improved version accommodates typical input ranges of 10, 50, and 100 V. The input termination can be single-ended or differential, with input resistance selectable among 50 Ω, 120 Ω, or 10 kΩ.

A trigger circuit continuously monitors the signals on all four channels, comparing the signal level on each channel with a predetermined threshold level. The threshold for each channel in the original version could be set at any level from 5 to 95 percent of full scale, independently of the threshold levels for the other channels; in the improved version, threshold can be set at any level between 1 and 99 percent. When the signal level in any channel exceeds its threshold level, a trigger signal is generated, causing full recording of data to begin simultaneously on all four channels.

Even when data are not being recorded fully, 12-bit analog-to-digital (A/D) converters in the four channels operate continuously, temporarily storing their output data in first-in/first-out (FIFO) registers that are always kept half full. When a trigger signal is received, the remaining halves of the FIFO registers are filled up with data. Inasmuch as the full capacity of each FIFO register corresponds to an observation interval of 200 μs, this arrangement provides a 100-μs pretrigger recording capability.

In the previous version, once a transient had been thus recorded, and during intervals of inactivity, the data were transferred to a nonvolatile memory. In the improved version, the data are transferred to both the nonvolatile memory and a second set of FIFO registers. The second FIFO set can be made as deep as needed to store as many waveforms as required. The design of the improved version makes it easy to replace either or both sets of FIFO registers to change record lengths and waveform storage capacities. The nonvolatile memory retains the data even if power is lost.

The previous version of the instrument was equipped with a clock, and the stored data were time-coded to establish the times of transients and to facilitate correlation with data on the same transients measured by other instruments. The improved version retains this internal clock, but is also equipped with a Global Positioning System (GPS) receiver and an Inter Range Instrumentation Group B (IRIG-B) decoder for accurate time stamping of any recorded waveform. If the IRIG-B signal is lost, the waveform is stamped with the time from the internal clock.

Like the previous version of the instrument, the present version is normally powered through an ordinary AC power line and includes backup batteries. During normal operation, the batteries are automatically charged. In the event of failure of AC power, the batteries can sustain operation for as long as 8 hours.

The design of the improved version is amenable to the addition of a cellular-telephone data link or other radio transceiver to enable remote interrogation of the status of the transient recorder or to retrieve data either on request or at scheduled intervals. For applications in which real-time retrieval of data is not feasible, one could use such other data-storage devices as rewriteable compact disk read-only memories (CD-ROMs). The introduction of CD-ROMs would increase the data-acquisition and -storage capacity from the current level of 16 waveforms to several tens of thousands of waveforms.

This work was done by Pedro J. Medelius of Dynacs Engineering Co., Inc., for **Kennedy Space Center**. *Further information is contained in a TSP [see page 1].*
KSC-12174

Books and Reports

The Future of Electronic Device Design

An article discusses anticipated advances in the design of increasingly capable integrated circuits containing ever smaller electronic devices. The article emphasizes the emergence of technology computer-aided design (TCAD) — a discipline in which computer-aided design is combined with computational simulation (based on underlying physics) of the operation and fabrication of devices. The article describes challenges that must be met to expand the role of TCAD as a means of overcoming obstacles to further miniaturization and of shortening integrated circuit development cycles. One challenge is to develop better mathematical

models of the device physics and fabrication processes to enable the more accurate simulation of what happens as circuit features shrink toward molecular dimensions; meeting this challenge will likely involve development of capabilities for "virtual fabrication," in which all aspects of production processes and devices produced could be computationally simulated. Another challenge is to develop new, generally applicable TCAD software with the flexibility and functionality needed to perform increasingly complex and accurate computations. A third challenge is to obtain the enormous computational power needed for advanced TCAD by setting up an Internet-based distributed computing grid, which would utilize thousands or even millions of computers while they were idle.

This work was done by Bryan A. Biegel of MRJ Technology Solutions, Inc., for **Ames Research Center**. *To obtain a copy of the article, "The Future of Electronic Device Design," see TSP's [page 1].*
ARC-14303

Electronic Systems

Hardware, Techniques, and Processes

12 BLANK PAGE

Current-Signature Sensor for Diagnosing Solenoid Valves

Changes in current signatures are indicators of electrical and mechanical deterioration.

John F. Kennedy Space Center, Florida

The "smart" current-signature sensor is an instrument that noninvasively measures and analyzes steady-state and transient components of the magnetic field of (and, thus, indirectly, the electric current in) a solenoid valve during normal operation. The instrument is being developed to enable continuous monitoring of integrity and operational status of solenoid valves without need for interrupting operation to conduct frequent inspections. The instrument is expected to be capable of warning of imminent solenoid valve failures so that preventive repairs can be performed. The basic instrument concept should also be adaptable to similar monitoring of electromechanical devices, other than solenoid valves, that are required to be highly reliable.

This current-signature sensor exploits the fact that unique characteristics (signatures) of the solenoid current — especially of the turn-on and turn-off current transitions — are affected by electrical and mechanical deterioration of the solenoid and valve parts. Current signatures include characteristic peaks and valleys (see figure) that repeat at well-defined times during every operating cycle and have well-defined magnitudes and shapes. As electrical and/or mechanical deterioration occurs, the peaks and valleys change both in time and magnitude; these changes can serve as indications of potential trouble.

The hardware portion of this current-signature sensor comprises a signal-acquisition assembly and a signal-conditioner/controller assembly. The signal-acquisition assembly contains a linear Hall-effect sensor for measuring the magnetic field generated by the current in the solenoid, plus a flux concentrator to maximize the response of the sensor and a shielding cage to prevent unwanted external magnetic fields from reaching the sensor. A temperature sensor is included to enable compensation for the temperature dependence of the response of the Hall-effect sensor.

The signal-conditioner/controller assembly includes an analog module, a microprocessor controller module, and a power-supply module. A real-time calibration module was being designed at the time of reporting the information for this article. The analog module conditions the low-level signal coming from the signal-acquisition assembly. The preamplification and final amplification stages in the analog module contain digitally controlled potentiometers that are used to compensate in real time for variations with temperature of the offset and gain components of the sensor and the signal-processing circuitry.

The settings for the digitally controlled potentiometers are provided by the microprocessor controller module. Prior to operation, calibration measurements with known inputs are taken at various temperatures to characterize the temperature dependence of the sensor and the signal-processing circuitry. A compensation curve is then calculated and programmed in the microprocessor controller module for use in the real-time temperature compensation as described above.

The real-time calibration module is envisioned to be connected to a calibration coil that would be part of the signal-acquisition assembly. Upon command

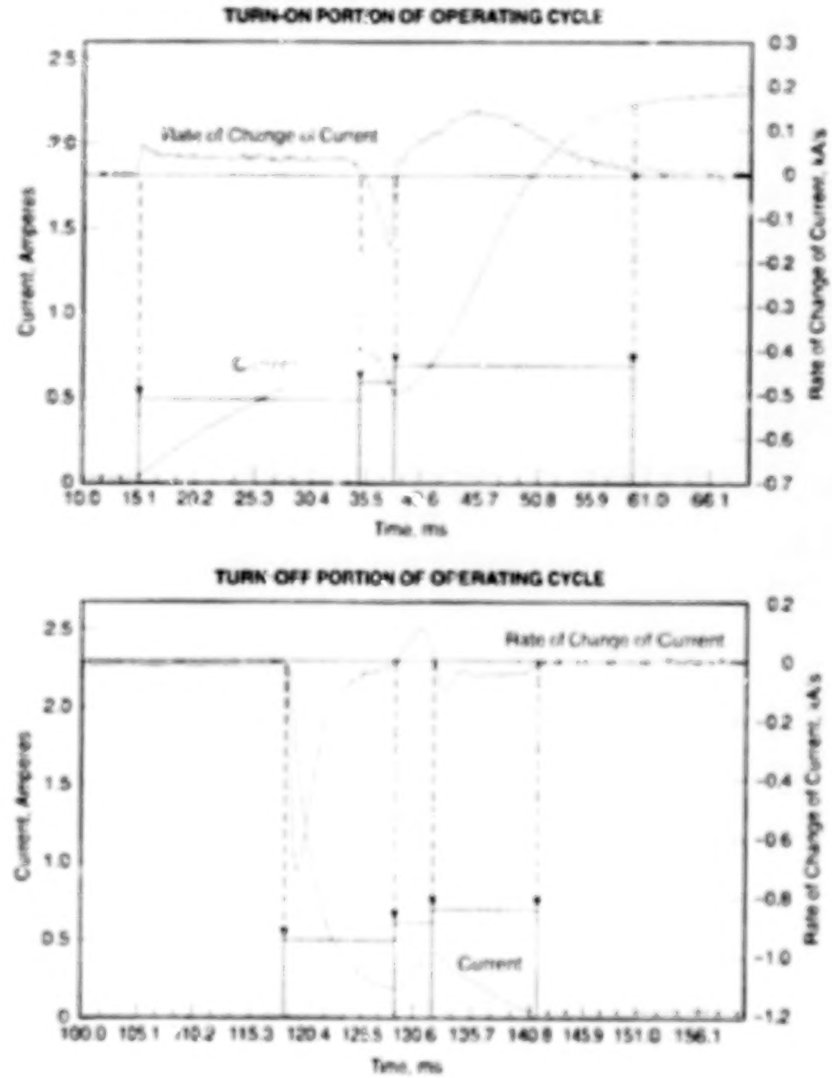

Characteristic Peaks and Valleys can be seen in the current and in the rate of change of the current in a solenoid at turn-on and turnoff.

by either the microprocessor controller module or a technician, the real-time calibration module would perform a complete sequence of calibration measurements to determine whether the sensor or other parts of the instrument had deteriorated.

In addition to temperature compensation, the microprocessor controller module is responsible for both real-time and trend analysis of the current signature. In operation, every valve cycle would be monitored and "health" parameters would be calculated to determine whether the monitored solenoid valve is performing within the nominal parameters. The "health" analysis and prediction of failure would be performed by software residing in the microprocessor controller module.

Thus far, a simple algorithm has been devised to detect specific characteristics of the current signal: A simple first derivative of the signal with respect to time (that is, the rate of change of the signal) would be calculated in real time. Peaks and valleys of the current signal would be detected and time-tagged by looking for zero crossings of the rate of change. Slope and steady-state values of the signal would also be monitored. These current-signature parameters would be compared against stored parameters and parameter-uncertainty ranges that would represent the behavior of a typical solenoid valve. The results of the comparisons would be summarized as indications of a nominal, border-line, or failure condition. An account of these results and of the statistics of nominal, border-line, and failure cycles would be stored as well as forwarded to a technician for further action.

This work was done by Jose M. Perotti, Angel R. Lucena, Curtis M. Ihlefeld, and Mario J. Bassignani of **Kennedy Space Center**. *Further information is contained in a TSP [see page 1].*

This invention is owned by NASA, and a patent application has been filed. Inquiries concerning nonexclusive or exclusive license for its commercial development should be addressed to the Technology Programs and Commercialization Office, Kennedy Space Center, (321) 867-6373. Refer to KSC-12152.

Closed-Loop Microsphere Laser for Optoelectronic Oscillator

Feedback control of the frequency of a pump laser is no longer necessary.

NASA's Jet Propulsion Laboratory, Pasadena, California

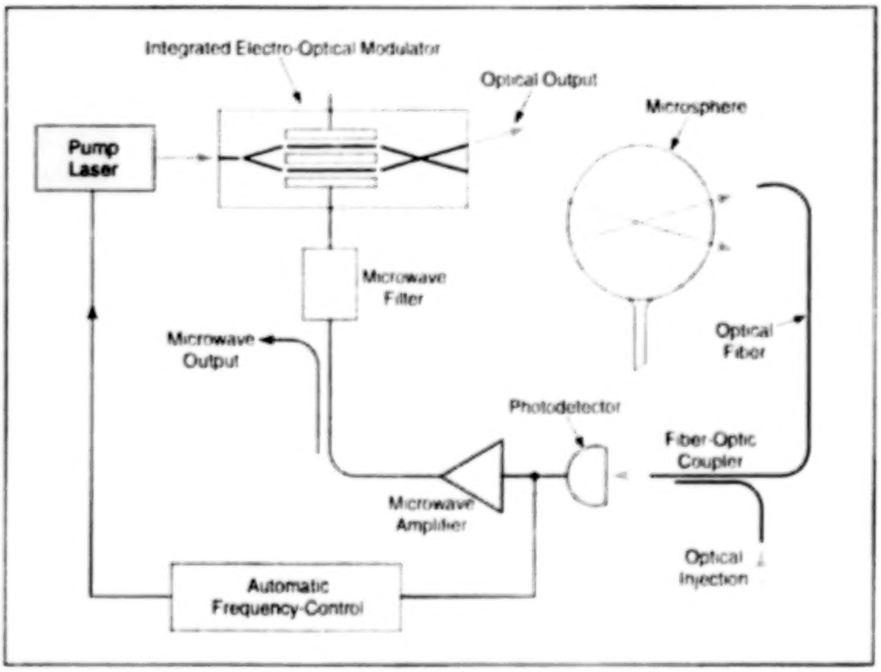

Figure 1. In the **Original Microsphere-Based Optoelectronic Oscillator**, an automatic frequency-control circuit was used to lock a pump laser to one of the electromagnetic modes of the microsphere.

A prototype ring laser in which a transparent microsphere serves as an electromagnetic-mode selector has been constructed in a continuing effort to develop optoelectronic oscillators for generating light signals amplitude modulated by microwave signals, all with low phase noise. Optoelectronic oscillators could be used as signal sources in fiber-optic and microwave communication systems and in radar systems.

An optoelectronic oscillator is a hybrid of photonic and electronic components, designed to exploit coupling between optical and electronic oscillations. Optoelectronic oscillators have been described in several previous articles in *NASA Tech Briefs*, the most recent being "Optoelectronic Generation of Optical and Microwave Signals" (NPO-20090), Vol. 22, No. 9 (September 1998), page 50. An optoelectronic oscillator includes, among other things, a laser that operates in multiple modes, plus a high-speed photodetector that samples the laser output. The laser is designed so that the frequency intervals between its modes include the microwave frequency of interest; thus, the microwave frequency of interest appears as one of the beat notes in the photodetector output.

In some previously developed optoelectronic oscillators, long fiber-optic feedback loops were used to obtain low phase noise. Undesirably, a long fiber-optic loop adds considerably to the size and weight of an oscillator; it also makes the frequency intervals between modes so small that selection of the desired modes becomes difficult. In some optoelectronic oscillators developed more recently, fiber-optic loops were replaced with transparent microspheres configured as high-Q (where Q is the resonance quality factor) resonators in conjunction with pump lasers operating under feedback control of frequency (see Figure 1). In a microsphere, propagation in a long fiber is replaced by equivalent orbiting of light by total internal reflection in "whispering-gallery" modes. It has been demonstrated experimentally that in visible light, $Q = 10^{?}$ can be achieved in a microsphere, corresponding to a propagation delay of about 3 μs in an optical fiber 0.7 km long.

Feedback control of pump-laser frequency in a microsphere oscillator of the type described above was necessary for locking

the pump laser to one of the microsphere modes. The feedback frequency control added complexity and introduced a source of additional frequency and phase noise.

In the prototype ring laser, there is no need for feedback control of laser frequency because the microsphere is an integral part of the laser. The prototype ring laser (shown in the upper part of Figure 2) includes a high-purity silica microsphere and a semiconductor optical amplifier plus ancillary optical components connected in an optical loop. One of the components in the loop is an optocoupler for sampling the laser beam.

In early experiments on the prototype ring laser, the sampled laser beam was analyzed for its optical and microwave-modulation spectral contents. The laser was found to oscillate in multiple whispering-gallery modes of the microsphere. The microwave modulation spectrum included peaks at integer multiples of the whispering-gallery free spectral range of 5.93 GHz. At the time of reporting the information for this article, experiments on the apparatus shown in the lower part of Figure 2 were underway. This apparatus is designed to obtain stable single-frequency operation by introducing (1) optical selection of principal waveguide modes and (2) active microwave feedback as in a standard optoelectronic oscillator.

This work was done by Steve Yao, Vladimir Iltchenko, and Lute Maleki of Caltech for **NASA's Jet Propulsion Laboratory**. *Further information is contained in a TSP [see page 1].*

In accordance with Public Law 96-517, the contractor has elected to retain title to this invention. Inquiries concerning rights for its commercial use should be addressed to

Technology Reporting Office
JPL
Mail Stop 249-103
4800 Oak Grove Drive
Pasadena, CA 91109
(818) 354-2240

Refer to NPO-20597, volume and number of this NASA Tech Briefs issue, and the page number.

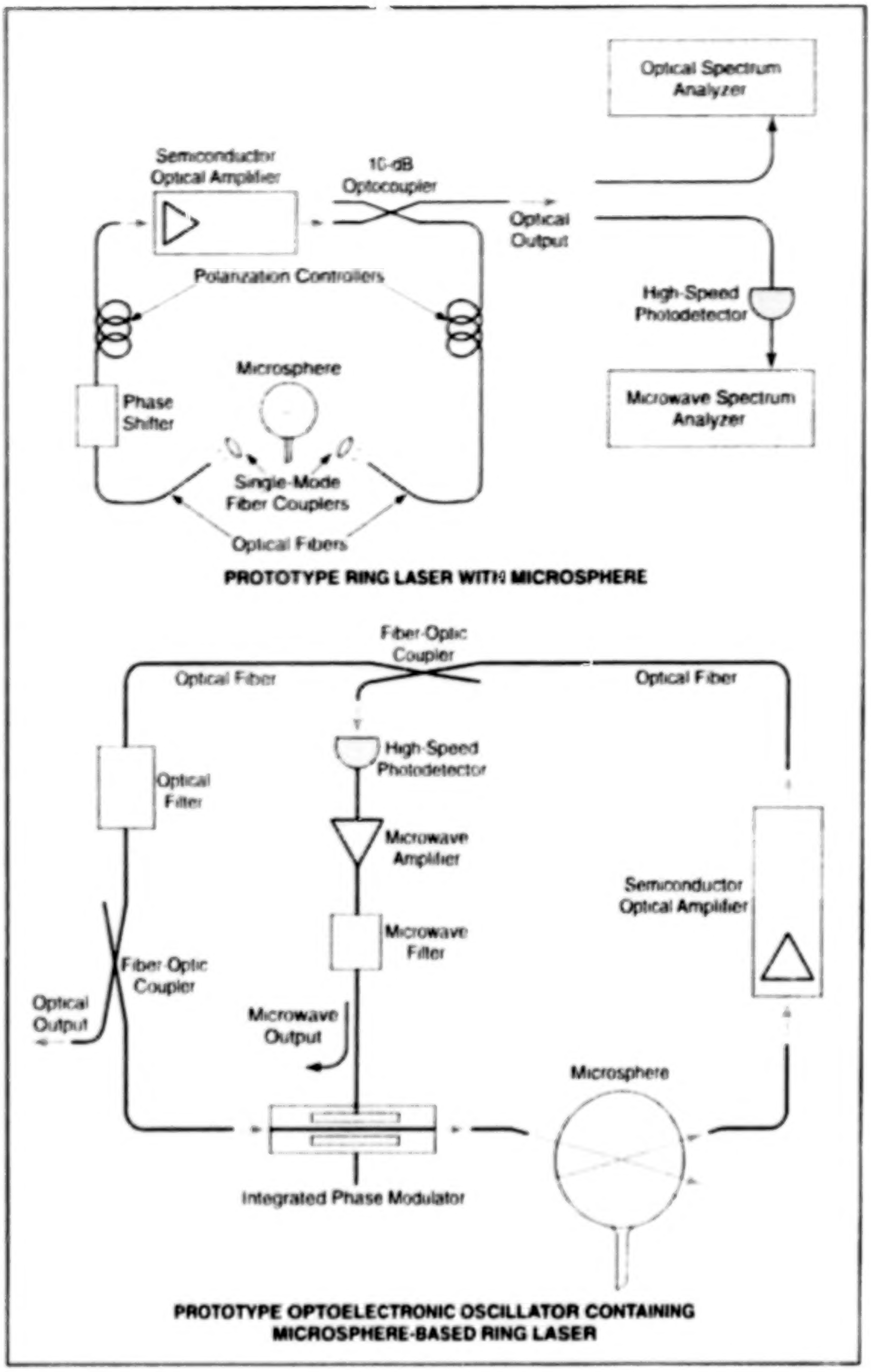

Figure 2. **Microsphere-Based Ring Lasers** have been built to demonstrate direct laser oscillation in microsphere modes, with microwave sidebands at integer multiples of the free spectral range of "whispering-gallery" microsphere modes.

Miniature Optoelectronic Oscillators Based on Microspheres

These oscillators could be highly miniaturized.

NASA's Jet Propulsion Laboratory, Pasadena, California

The figure depicts an example of a proposed type of optoelectronic oscillator (OEO) based on some of the same principles as those described in the preceding article. In the proposed OEOs as in the OEOs of the preceding article, transparent (e.g., glass) microspheres that exhibit "whispering-gallery" electromagnetic modes at the laser wavelengths of the oscillators would be utilized as high-Q (where Q is the resonance quality factor and is the measure of energy storage time) resonator/delay elements in the oscillator feedback loops.

The microspheres, which have submillimeter diameters, would replace the fiber-optic delay lines that have been used in previously developed OEOs. A typical fiber-optic delay line is of the order of 1 km long and is wound on a spool about 3 cm in diameter and 5 cm long. The proposed OEOs could readily be miniaturized

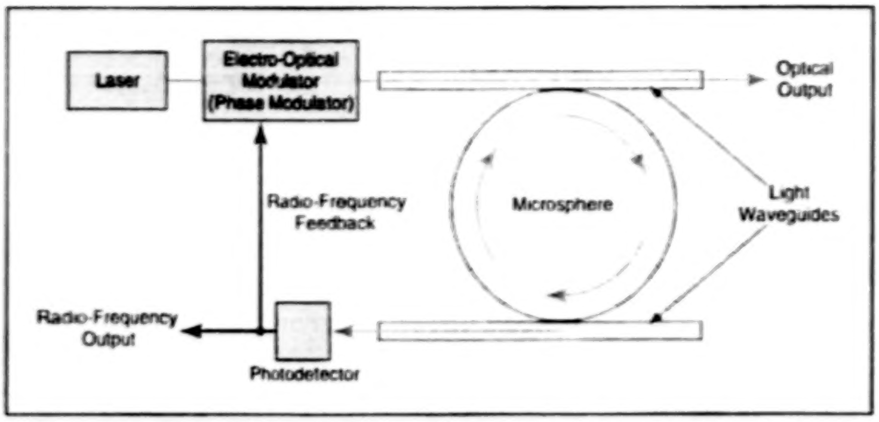

A Microsphere Would Be Incorporated into the feedback loop of an optoelectronic oscillator.

because, in the absence of the bulky fiber-optic delay lines, all of their otherwise microscopic optical and electronic components could be integrated on single chips.

In a microsphere, propagation in a long fiber is replaced by equivalent circulation of light by total internal reflection in "whispering-gallery" modes. This light propagates in equatorial planes near the surface. It has been demonstrated experimentally that $Q = 10^{10}$ can be achieved in a glass microsphere, limited only by absorption of light in the glass.

In the OEO shown in the figure, the microsphere would be incorporated into the oscillator feedback loop via evanescent-wave coupling with optical waveguides. In one operational scenario, light from the output of a phase modulator would be coupled into the microsphere to excite two modes, corresponding to a carrier signal and a sideband; it would be possible to do this because deviations from perfect sphericity would create modes with a frequency difference falling in the microwave range. The beat note between the two modes would appear at the output of the photodetector and would constitute the desired microwave signal. Some of the beat-note power would be fed back to the modulator to sustain the oscillation.

This work was done by Lute Maleki, Steve Yao, and Vladimir Iltchenko of Caltech for **NASA's Jet Propulsion Laboratory**. *Further information is contained in a TSP [see page 1].*

In accordance with Public Law 96-517, the contractor has elected to retain title to this invention. Inquiries concerning rights for its commercial use should be addressed to

Intellectual Property group
JPL
Mail Stop 202-233
4800 Oak Grove Drive
Pasadena, CA 91109
(818) 354-2240

Refer to NPO-20592, volume and number of this NASA Tech Briefs *issue, and the page number.*

Optoelectronic Oscillators Based on Fiber-Optic Resonators

Relatively compact resonators would replace long delay lines.

NASA's Jet Propulsion Laboratory, Pasadena, California

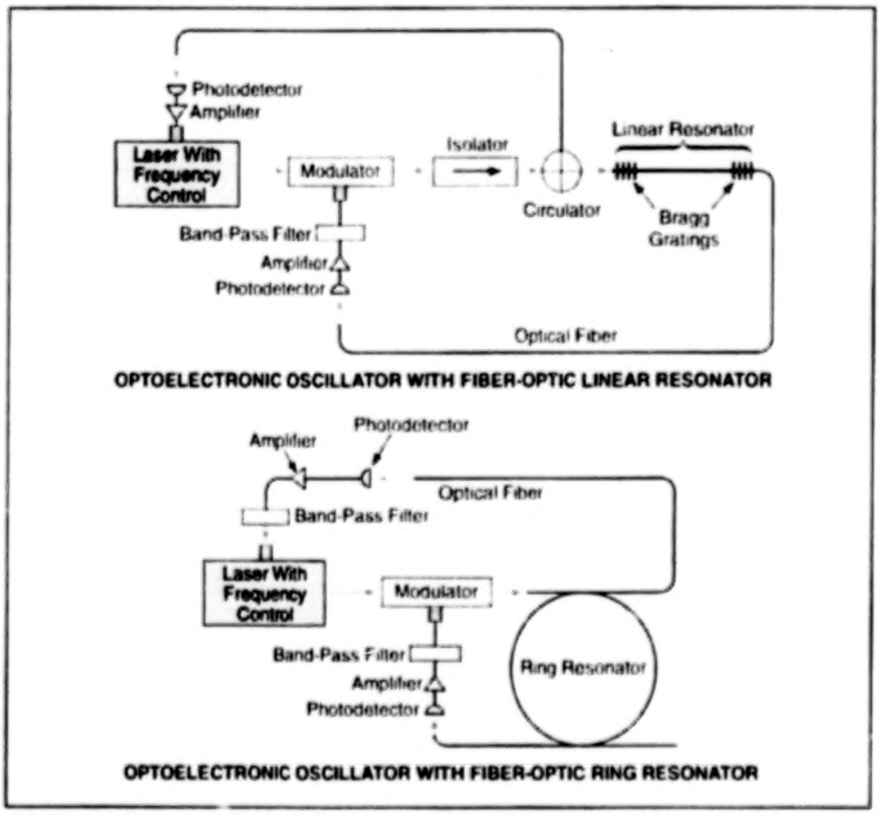

OEOs Could Contain Fiber-Optic Linear or Ring Resonators, instead of long fiber-optic delay lines.

Optoelectronic oscillators (OEOs) of a proposed type would be based partly on the use of fiber-optic linear or ring resonators in place of the long fiber-optic delay lines that have been used to obtain low phase noise in some previously developed OEOs. Although the proposal to use fiber-optic linear or ring resonators was made prior to the use of microsphere resonators described in the two preceding articles, this article appears as the third in the series because the two microsphere-related articles provide information that is prerequisite for appreciating the technical significance of the proposal.

The two preceding articles discuss two of the disadvantages of long fiber-optic delay lines; excessive weight and size, plus difficulty of selecting desired electromagnetic modes because of smallness of frequency intervals between modes. Two more disadvantages arise in conjunction with the need to prevent temperature-induced frequency drift: (1) it is difficult to stabilize the temperature on a long optical fiber, even when the fiber is coiled on a spool, and (2) optical fibers with low thermal expansion are expensive.

The figure illustrates an OEO with a fiber-optic linear resonator and one with a fiber-optic ring resonator. In the case of the linear resonator, the ends of the resonating length would be defined by Bragg gratings or, alternatively, by highly reflective coatings at the ends of the fiber. In the case of a linear resonator, light would propagate with multiple reflections from the ends; in the case of a ring resonator, light would propagate around the ring many times. Thus, in either case, the effective length of the resonator would be greater than the simple geometric length or circumference.

In either case, the frequency interval between modes would equal the free spectral range of the resonator. In order to obtain oscillation, the frequency of the laser carrier signal must equal that of a resonator mode; the frequencies of the laser-beam modulation sidebands must also equal frequencies of other resonator modes. To provide the necessary alignment of frequencies, the laser frequency must be stabilized at a peak of the resonator transmission spectrum. This can be accomplished by a feedback control subsystem that continually monitors the power of light reflected from the resonator and responds by adjusting the laser frequency to drive the reflected power toward a minimum.

If the resonator could be stabilized, then the absolute frequency of the laser would thus be stabilized. Taking advantage of the relatively small amount of fiber needed to achieve a large effective length, one could then fabricate the resonator from low-thermal-expansion fiber.

This work was done by Steve Yao and Lute Maleki of Caltech for **NASA's Jet Propulsion Laboratory**. *Further information is contained in a TSP [see page 1].*

In accordance with Public Law 96-517, the contractor has elected to retain title to this invention. Inquiries concerning rights for its commercial use should be addressed to

Technology Reporting Office
JPL
Mail Stop 249-103
4800 Oak Grove Drive
Pasadena, CA 91109
(818) 354-2240

Refer to NPO-20547, volume and number of this NASA Tech Briefs issue, and the page number.

Physical Sciences

Hardware, Techniques, and Processes

Books and Reports

20

BLANK PAGE

Photonic Switching Devices Using Light Bullets

Light bullets would be used to deflect each other.

Ames Research Center, Moffett Field, California

A class of proposed photonic switching devices would utilize interactions among light bullets that have been studied theoretically. Because they function at speeds much greater than those of electrically, magnetically, and acoustically actuated switching devices, these and other photonic switching devices are attracting increasing attention as potential solutions to the problems of switching in the development of advanced communication networks, signal-processing systems, and digital computers.

The concept of a light bullet is a special case of the more general concept of a soliton. A light bullet is a small pulse of light that, in a suitable optically nonlinear material, retains its shape and is guided along its path of propagation by virtue of a balance among diffraction, group velocity dispersion, and nonlinear self phase modulation. To be suitable for supporting light bullets, a material should have a negative group-velocity dispersion and a sufficiently large nonlinear index of refraction.

Computational simulations have shown that two counterpropagating light bullets that approach each other within approximately the width of one of them would attract each other enough to change their directions of propagation by appreciable amounts. This phenomenon would be exploited to effect switching in the proposed devices. The figure schematically depicts a typical proposed device comprising a rectangular slab waveguide with multiple input/output channels at both ends. In one example, a light bullet would enter along a horizontal path through a central channel (channel C) simultaneously with another light bullet entering along a slightly laterally displaced horizontal path through the opposing central channel (channel H). Upon passing each other near the middle, the two light bullets would attract each other, causing the upper one to be deflected onto a downward slant and the lower one to be deflected onto an upward slant. The amount of attraction would increase with the intensity of either light bullet and would decrease with increasing lateral separation. Hence, by suitable choice of the intensities and the lateral separation between entry paths, one could cause the light bullets to travel to chosen output channels (A or B for the leftward-propagating light bullet, and I or J for the rightward propagating bullet). Of course, if no light bullet were to enter through channel H, then the light bullet entering through channel C would propagate without deflection and leave through channel H.

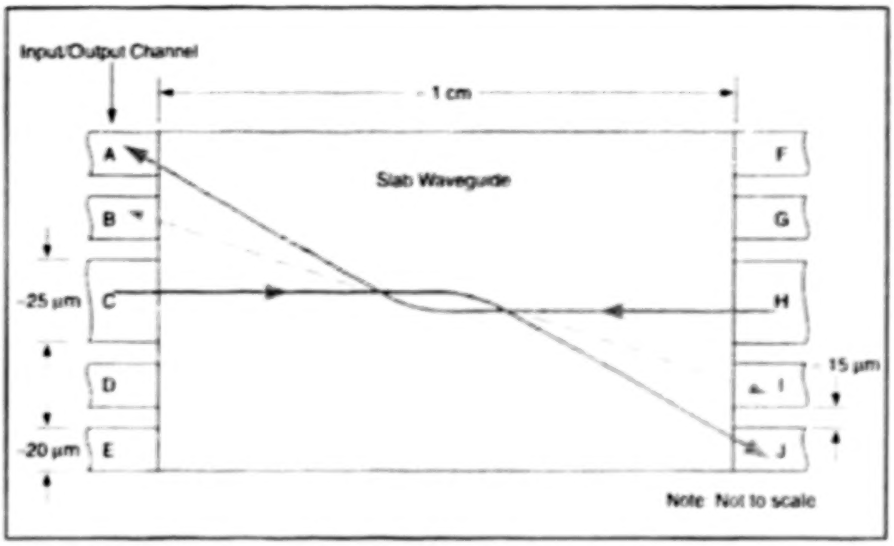

Light Bullets Entering Through Opposing Channels would pass close to each other near the middle, where an attraction between them would deflect them to desired output channels. The dimensions shown here are for the example of doped glass described in the text. The dimensions would scale with the proposed nonlinear material.

There are many potential variations on the basic theme described above. For example, one light bullet could be made to enter horizontally through channel C and the other light bullet made to enter through channel I at a slant chosen to make the two light bullets pass near each other, deflecting each other to chosen output channels. Yet another variation would be to time the entering light bullets so that they would meet at a location other than the middle, the location being chosen in conjunction with the intensities and the lateral displacement to deflect the light bullets to the desired output channels.

A proposed material for a device like that shown in the figure is a commercial doped glass that has a nonlinear index of refraction of 1.11×10^{-14} cm^2/W and a group velocity dispersion of −220 ps^2/km for light at a wavelength of ≈3.5 µm. It is estimated that this material would handle light bullets with a duration of ≈100 fs. The light bullets would be ≈10 µm wide in the plane of the figure, with a thickness about equal to that of the waveguide slab (≈2 µm).

The peak power needed to obtain a nonlinear effect strong enough to support a light bullet is an important consideration in designing a practical photonic switching device of this type. The peak power needed in this theoretical example has been estimated to be 150 kW. At a duration of 100 fs, the corresponding energy in a light bullet would be 15 nJ. These power and energy parameters are within the capability of currently available lasers.

However, it may be possible to reduce the power and energy requirements through the choice of a different nonlinear optical material. For example, the estimated required peak pulse power for a suitable semiconductor nonlinear optical material would be about 15 kW. The required power might be reduced even more sharply by use of multiple-quantum-well semiconductor structures: it has been estimated that such a structure might support the propagation of a light bullet at a peak power of only about 0.01 W.

This work was done by Peter M. Goorjian of **Ames Research Center**. *Further information is contained in a TSP [see page 1].*

This invention has been patented by NASA (U.S. Patent Nos. 5,963,683 and 5,651,079). Inquiries concerning nonexclusive or exclusive license for its commercial development should be addressed to the Patent Counsel, Ames Research Center, (650) 604-5104. Refer to ARC-14057.

Built-in "Health Check" for Pressure Transducers

Calibrations could be verified approximately, without removing transducers to calibration laboratories.

John F. Kennedy Space Center, Florida

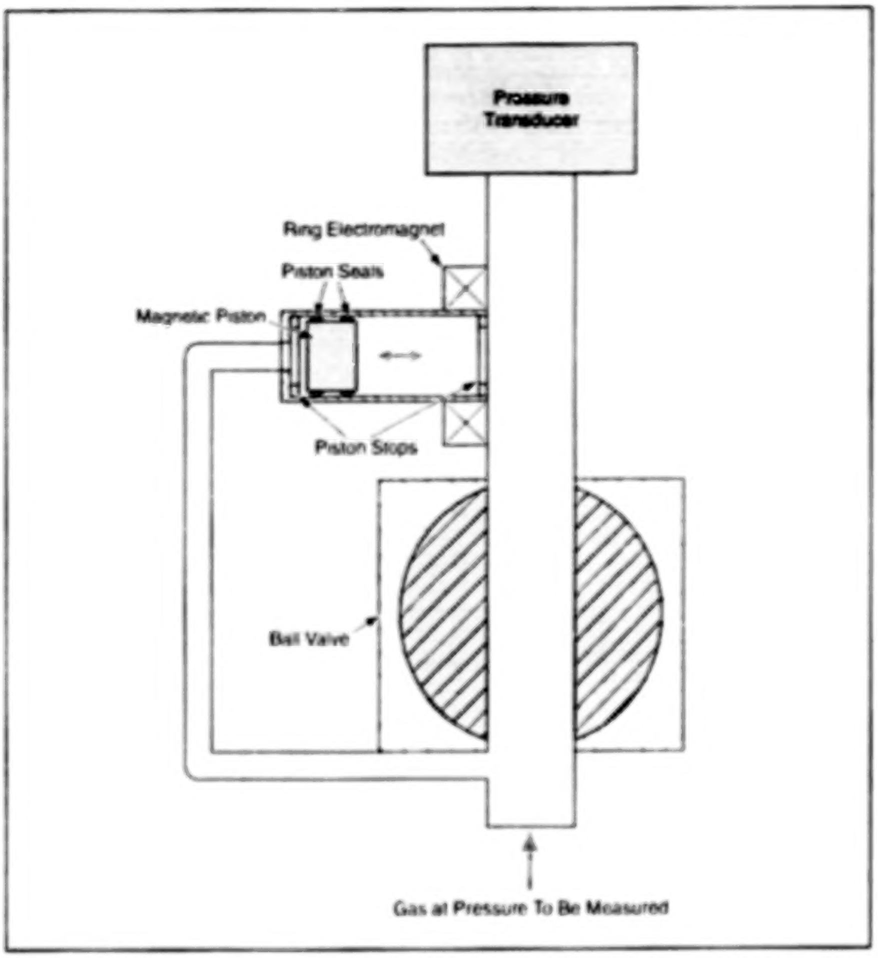

Figure 1. **The Volume of Gas** trapped between the piston and the ball valve would be known and would change by a known amount when the piston was actuated by the ring electromagnet.

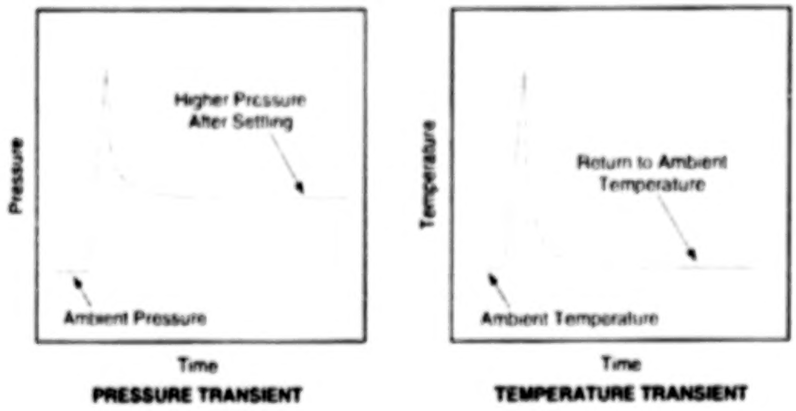

Figure 2. **Transient Decays of Pressure and Temperature** occur immediately after the compression stroke of the piston. The pressure settles to a steady higher value, while the temperature returns to the ambient value.

"Health check" would be built into pressure transducers, according to a proposal, to enable occasional, rapid, *in situ* testing of the transducers between normal pressure-measurement operations. The health check would include relatively simple devices that, upon command, would provide known stimuli to the transducers. The responses of the pressure transducers to these stimuli would be analyzed to quantify (at least approximately) deviations from the responses expected from previous rigorous calibrations. On the basis of such an analysis, a given pressure transducer could be removed from service, rigorously recalibrated, or continued in use with corrections applied for calibration drift. The use of the health check could provide timely warnings of pressure-transducer malfunctions and make it possible to retain confidence in the calibrations of pressure transducers while reducing the frequency with which they are replaced or subjected to full laboratory recalibration.

A pressure transducer health check would typically include (1) a circuit that would, on command, insert a shunt calibration resistor in a bridge circuit within which the pressure transducer normally functions, (2) a device that would compress or expand a known amount of trapped gas to effect an increase or decrease of input pressure, and (3) optionally, a gas-temperature transducer. The health check must be subjected to an initial rigorous calibration along with the pressure transducer.

During the operation of the health check, the change in the output voltage of the bridge circuit occasioned by the connection or disconnection of the shunt resistor would be measured and compared with the corresponding change in voltage measured during the rigorous calibration. Any difference between these voltage changes would be attributed to a change in sensitivity of the pressure transducer or, equivalently, in the amplification in its signal-processing circuitry.

Figure 1 depicts the compression/expansion portion of the health check device installed on the input tube of a typical pressure transducer. To perform a health check, first the pressure transducer would be exposed to ambient pressure, then a ball valve would be actuated to trap gas in the pressure transducer, then a piston would be actuated by an electromagnet to change the volume of the trapped gas. A first pressure-transducer reading would be taken before the piston stroke; a second pressure-transducer reading would be taken long enough after the stroke that any measur-

able transient heating from compression or transient cooling from rarefaction would have dissipated, but not so long after actuation that the ambient temperature would have changed. By use of Boyle's law, the actual pressure after the piston stroke could be calculated from the ambient pressure and the ratio between the volumes, which would have been determined in the rigorous calibration. Pressure-transducer readings taken over several cycles of exposure to ambient pressure, compression, and rarefaction could be analyzed to determine any deviations from calibration and to characterize the response of the pressure transducer with respect to repeatability, hysteresis, and linearity.

The inclusion of a gas temperature transducer would make it possible to extract additional information from the decay of the temperature transient that follows the piston stroke (see Figure 2). One would measure the temperature at intervals much smaller than the characteristic time of the temperature transient and would then attempt to fit the measured temperatures to a decaying exponential.

The reason for attempting this fit is that to a first approximation, the temperature of the gas would decay exponentially toward the ambient temperature with a characteristic time

$$\tau = mc_v/hA,$$

where m is the mass of the trapped gas, c_v is the specific heat of the gas at constant volume, h is a heat-transfer coefficient, and A is the total area of all surfaces that enclose the trapped gas. The value of c_v is known and the values of h and A would be determined during the rigorous calibration. Fitting the temperature measurements to an exponential would provide the value of τ, from which one could calculate m.

Using m, the known volume of the container, and the ideal gas law or any other equation of state that is appropriate, one could calculate the pressure of the trapped gas as a function of temperature. This calculation would provide an additional calibration of the pressure transducer against the temperature transducer, making it possible to use the temperature transducer to perform an additional health check.

If either the pressure or the temperature transducer were malfunctioning and it could be determined which was malfunctioning, then by use of the ideal gas law, one could still estimate the pressure or temperature from the temperature or pressure reading, respectively. As another health check, if either the temperature or the pressure measurements during the transient were to fit a decaying exponential poorly, then the temperature or pressure transducer, respectively, could be assumed to be responding nonlinearly and malfunctioning. As yet another health check, temperature and pressure readings could be compared through the equation of state to determine whether there was an offset error in the output of one of the transducers (though it would not be possible to determine which had the offset).

This work was done by Richard T. Deyoe, Pedro Medelius, Christopher Immer, Stanley Starr, and Anthony Eckhoff of Dynacs Engineering Co., Inc., for **Kennedy Space Center**. *Further information is contained in a TSP [see page 1].*

This invention is owned by NASA, and a patent application has been filed. Inquiries concerning nonexclusive or exclusive license for its commercial development should be addressed to the Technology Programs and Commercialization Office, Kennedy Space Center, (321) 867-4879. Refer to KSC-12139/12077.

Books and Reports

All-Pressure Fluid-Drop Model Applied to a Binary Mixture

A report presents a computational study of the subcritical and supercritical behaviors of a drop of heptane surrounded by nitrogen, using the fluid-drop model described in "Model of a Drop of O_2 Surrounded by H_2 at High Pressure" (NPO-20220) and "The Lewis Number Under Supercritical Conditions" (NPO-20256), *NASA Tech Briefs*, Vol. 23, No. 3 (March 1999), pages 66-70. In this model, the differences between subcritical and supercritical behaviors are identified with length scales. The report compares results of the computations with data from microgravity experiments on large drops at temperatures and pressures in the sub- and supercritical regimes. The maximum rate of regression of the drop diameter (defined as the diameter of maximum density gradient) is found to be well predicted at all pressures. Computations for a small drop and for the case of a transient pressure that crosses the critical point are analyzed and major differences between sub- and supercritical behaviors are explained. In particular, it is shown that the classical calculation of the Lewis number gives erroneous results at supercritical conditions, and that an effective Lewis number in the model correctly estimates the length scales for heat and mass transfer at all pressures.

This work was done by Josette Bellan and Kenneth Harstad of Caltech for **NASA's Jet Propulsion Laboratory**. *To obtain a copy of the report, "An All-Pressure Fluid Drop Model Applied to a Binary Mixture: Heptane in Nitrogen," see TSP's [page 1].*
NPO-20701

Validation of All-Pressure Fluid-Drop Model

A report presents a computational study of the subcritical and supercritical behaviors of a drop of heptane surrounded by nitrogen. The subject matter is basically same as that of the report described in the preceding article, except that the Lewis-number issue is not addressed in detail; however, this article presents the full set of equations which lack in the former. As in the preceding case, the results of the computations are compared with data from microgravity experiments on drops of heptane evaporating in nitrogen at temperatures and pressures in the sub- and supercritical regimes, and conclusions are drawn regarding the accuracy of (1) the mathematical model used in the present study and (2) the limitation on accuracy of a traditional model (known as the d^2 law) at supercritical pressures. The conclusions stated in the report are essentially a subset of the conclusions stated in the report described in the preceding article.

This work was done by Josette Bellan and Kenneth Harstad of Caltech for **NASA's Jet Propulsion Laboratory**. *To obtain a copy of the report, "Validation of an All-Pressure Fluid Drop Model: Heptane Fluid Drops in Nitrogen," see TSP's [page 1].*
NPO-20707

Validated Model of a Fluid Drop for All Pressures

The report "A Validated All-Pressure Fluid Drop Model and Lewis Number Effects for a Binary Mixture" presents one in a series of theoretical and computational studies of the subcritical and supercritical behaviors of a drop of fluid and, in particular, a drop of heptane surrounded by nitrogen. The study is based on a fluid

drop model in which, among other things, the differences between subcritical and supercritical behaviors are identified with length scales. It is shown that in the subcritical regime and for a large rate of evaporation from the drop, there exists a mass-fraction "film layer" immediately below the drop surface and the solution of the model equations has a convective-diffusive character. In the supercritical regime, there is no material surface to follow, and this introduces an indeterminacy in the boundary conditions. To resolve the indeterminacy, one must follow an arbitrary boundary, which, in this case, is that of the initial fluid drop. The solution has then a purely diffusive character, and from this solution, one calculates the location of the highest density gradient, which location is identified with the optically observable boundary. It is also shown that the classical calculation of the Lewis number gives qualitatively erroneous results at supercritical conditions, but that an effective Lewis number previously defined gives qualitatively correct estimates of the length scales for heat and mass transfer at all pressures.

This work was done by Josette Bellan and Kenneth Harstad of Caltech for **NASA's Jet Propulsion Laboratory**. *To obtain a copy of the report, see TSP's [page 1].*
NPO-20702

Subgrid Analysis of Mixing Layer With Evaporating Droplets

This report presents an analysis of a database from computational simulations of a droplet-laden mixing layer (i.e., evaporating droplets of a liquid fuel in air) undergoing a transition to turbulence. The basic governing equations were those of transport of discrete droplets through a flowing gas; the droplets were followed in a Lagrangian frame whereas the gas was followed in an Eulerian frame. The analysis involved the extraction of subgrid scale (SGS) models from flow fields generated using the direct numerical simulation (DNS) approach, in which the governing equations are solved directly at all relevant length scales. The SGS models are intended for use in a large-eddy simulation (LES) approach, in which the governing equations are approximated such that the flow field is spatially filtered and subgrid phenomena are represented by arbitrary mathematical models. In the analysis, it was found that the gas-phase variables at the droplet locations were best modeled as the sums of (1) the filtered gas-phase variables at the grid points and (2) corrections computed from the filtered flow field in the same matter as SGS standard deviations. The SGS standard deviations were obtained, alternately, from the Smagorinsky, gradient, and scale-similarity models. When a proportionality factor inherent in the gradient and scale-similarity models was properly calculated by use of the DNS database, these models yielded results in excellent agreement with the DNS, while the Smagorinsky model proved inadequate.

This work was done by Josette Bellan and Nora Okong'o of Caltech for **NASA's Jet Propulsion Laboratory**. *To obtain a copy of the report, "A Priori Subgrid Analysis of Temporal Mixing Layers with Evaporating Droplets," see TSP's [page 1].*
NPO-20791

Materials

Hardware, Techniques, and Processes

Books and Reports

26 BLANK PAGE

Predicting Stresses in Thermal-Barrier Coatings

Creep, oxidation, differential thermal expansion, and interface roughness are taken into account.

John H. Glenn Research Center, Cleveland, Ohio

A methodology for predicting stresses and the resultant cracking in plasma-sprayed thermal-barrier coatings (TBCs) has been developed. The methodology is built around a computer code that implements a finite-element model that simulates the evolution of stresses, strains, and related phenomena in a TBC. The economic and technological value of the methodology lies in its potential to provide a more systematic basis for designing reliable and durable TBCs for advanced gas turbine engines by reducing the amount of time-consuming empirical testing needed to assess alternative TBC designs.

A TBC typically comprises a ceramic top coat deposited on an alloy bond coat that has been deposited on a superalloy substrate that the TBC is intended to protect. Together, the TBC and the substrate constitute a complex material system. Finite-element modeling is necessary to predict the complex, interactive thermomechanical and chemical behaviors of the component material layers.

The present finite-element model is capable of making such predictions over a range of conditions to which TBCs are exposed during operation of engines and during thermal cycling in burner test rigs. Originally developed within the framework of the Lawrence Livermore National Laboratory code NIKE2D, the model has recently been implemented into a new framework using the commercial FEA code ABAQUS™, a product of Hibbitt, Karlsson & Sorensen, Inc. Variable phenomena that are represented in the model include transient thermal behavior, multiple thermal cycles, and oxidation of the bond coat. The initiation of fractures and the propagation of cracks are represented by a stress-based crack-initiation criterion and a fracture-mechanics submodel. The creep behavior of each constituent material is represented by a temperature-dependent power-law creep submodel.

Oxidation of the bond coat is represented by use of provisions within the codes that allow for the transformation of constituent materials. The bond-coat oxide starts at the bond-coat/top-coat interface and grows into the thickness of the bond coat. In the model, on the basis of empirical data on the rate of growth of an oxide layer on a bond-coat material, bond-coat-alloy finite elements are replaced by bond-coat-oxide finite elements at fixed intervals of time, starting at the bond-coat/top-coat interface.

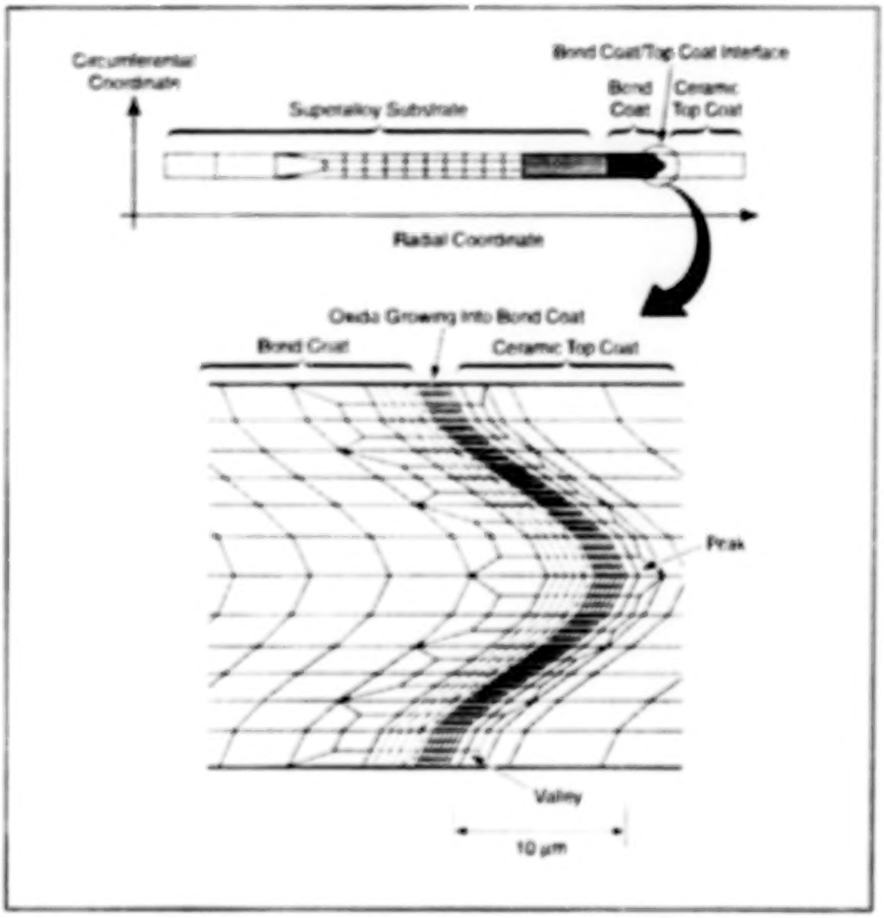

This **Small Part of the Finite-Element Model** shows the geometric relationships of the various layers and the simulation of surface roughness by use of a sinusoidal waviness.

The model can be used to assess the effects of numerous material, process, or geometric variables on the stress behavior within a TBC. Five principal variables originally studied and characterized during model development were oxidation, bond-coat creep, top-coat creep, bond-coat thermal expansion, and interfacial roughness. The outputs of the model include stresses as functions of time, location, and direction. The model has been applied to a burner-rig specimen, which is a 25.4-mm-diameter rod of Waspaloy (or equivalent superalloy) with a side TBC composed of 0.13-mm-thick NiCrAlY bond coat and a 0.25-mm-thick top coat comprised of a mixture of zirconia with 8 weight percent yttria. To simulate the effect of surface roughness of a typical TBC, the radial coordinate of the bond-coat/top-coat interface was made to vary as a sinusoidal function of the circumferential coordinate, with a peak-to-valley amplitude of 10 µm (see figure).

The numerical results of the application have been interpreted as signifying that oxidation of the bond coat exerts a strong effect on stresses in the ceramic layer and that stresses induced by oxidation are influenced by other factors, including bond-coat creep, top-coat creep and bond-coat roughness. It was also concluded that the progression of cracking is a result of the combined action of creep, oxidation, and thermal cycling. An accurate description of the entire process requires a model including these factors. It was further concluded that as complex as the model is, it is still too simple to provide a complete description of the failure of a TBC, and that for greater accuracy, it would be necessary to account for such other factors as (1) sintering phase changes in

the oxide, bond coat, and ceramic layers and (2) cracking and changes in composition in the ceramic layer.

This work was done by Andrew Freborg and B. Lynn Ferguson of Deformation Control Technology, Inc., for **Glenn Research Center**. *Further information is contained in a TSP [see page 1].*

Inquiries concerning rights for the commercial use of this invention should be addressed to NASA Glenn Research Center, Commercial Technology Office, Attn: Steve Fedor, Mail Stop 4–8, 21000 Brookpark Road, Cleveland, Ohio 44135. Refer to LEW-16783.

Enhancing the Removal of Chlorocarbons From Groundwater

Sonication apparently removes corrosion products that inhibit dechlorination.

John F. Kennedy Space Center, Florida

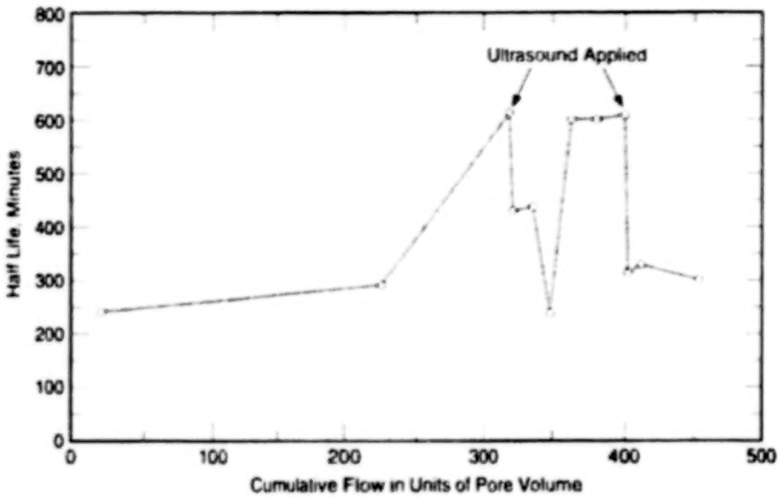

The **Half Life of Trichloroethane** in water flowing through a column filled with 50-mesh iron initially increased with time; that is, the column performance deteriorated. The subsequent application of ultrasound on two occasions caused sharp decreases in half life; that is, sonication restored column performance.

Experiments have shown that ultrasound could be an effective means of enhancing the removal of chlorinated hydrocarbon contaminants from groundwater by the zero-valent-metal treatment process. This process, which has been a subject of research in recent years, is attractive because it does not involve above-ground treatment or the use of pumps, and because the materials needed to effect treatment are safe and relatively inexpensive.

The process involves the use of a permeable wall that contains a metal (iron or zinc) in zero-valent condition and in porous form (e.g., dust or filings) and is buried in the ground. The position and orientation of the wall are chosen to take advantage of the natural groundwater gradient to carry the groundwater through the wall. As the contaminated groundwater flows through the wall, chlorine is removed from chlorinated hydrocarbons and from breakdown byproducts. The dechlorination reaction mechanism, which is not known precisely, appears to involve the simultaneous oxidation of metal and dechlorination of chlorinated hydrocarbons. For example, the removal of trichloroethane by treatment with iron appears to include the reactions:

$$Fe \rightarrow Fe^{2+} + 2e^- \text{ and } C_2HCl_3 + 3H^+ + 6e^- \rightarrow C_2H_4 + 3Cl^-.$$

Thus, the destruction of one mole of trichloroethane yields three moles of chloride and results in an increase in pH because of the consumption of protons. In addition, corrosion of iron is inherently part of the electron-transfer process that drives the dechlorination. The rate of dechlorination by a treatment wall decreases with time, apparently because the precipitation of corrosion products reduces the iron surface area accessible for dechlorination. In some cases, the rate of dechlorination could be reduced further because accumulation of corrosion products in pores could reduce the permeability of the wall.

The foregoing observations lead to the concept of using ultrasound to enhance treatment. It has been postulated that ultrasound can be used to remove corrosion products from iron surfaces and therefore can be used to restore and maintain rates of dechlorination. Results of batch and column-flow experiments confirm that exposure to ultrasound increases dechlorination rates significantly (see figure). Further experimental studies would be needed to develop a full-scale, practical ultrasonic system to enhance the function of a full-scale treatment wall.

This work was done by Jacqueline Quinn of **Kennedy Space Center** *and Nancy E. Ruiz, Debra R. Reinhart, Cherie L. Geiger, and Christian A. Clausen III of the University of Central Florida. Further information is contained in a TSP [see page 1].*

This invention is owned by NASA, and a patent application has been filed. Inquiries concerning nonexclusive or exclusive license for its commercial development should be addressed to the Technology Programs and Commercialization Office, Kennedy Space Center, (321) 867-6373. Refer to KSC-11959.

Books and Reports

Study of High-Performance Polyimide Foams

This report describes an experimental study of thermal stability, mechanical, and flammability properties of foams of several different densities made of three different polyimides. The study was performed because (1) prior such studies were performed on polyimide films rather than foams and (2) the synthesis of polyimide foams is a relatively recent development. There is a need to determine the suitability of each foam for potential applications — for example, as flame retarders, thermal and acoustic insulators, gaskets, seals, vibration-damping pads, spacers in adhesives and sealants, extenders, and flow and leveling aids. Analysis of experimental data acquired in the study led to the conclusions that the polyimide foams can be classified as high performance materials with respect to their mechanical and thermal stability properties and that they can

be regarded as fire-resistant even though the large surface areas of foams would ordinarily be expected to make fire retardance difficult to achieve. Differences among the surface areas or cell sizes of the foams were found to affect flammability properties more strongly than do differences in densities or chemical structures. However, it was also concluded that chemical structures may dictate surface areas or porosities in the formation of foams.

This work was done by Erik S. Weiser and Terry L. St. Clair of **Langley Research Center**, *Martha K. Williams of Kennedy Space Center, and Gordon L. Nelson and James R. Brenner of Florida Institute of Technology. To obtain a copy of the report, "High-Performance Polyimide Foams," see TSP's [page 1].*

This invention has been patented by NASA (U.S. Patent Nos. 6,133,330 and 6,180,746). Inquiries concerning nonexclusive or exclusive license for its commercial development should be addressed to Gregory S. Manuel at (757) 864-2556 or g.s.manuel@larc.nasa.gov. Refer to LAR-15977/15767.

Multi-Shock Blankets for Protecting Spacecraft

A report discusses multi-shock blankets, which are under investigation for use in protecting spacecraft against orbiting debris from prior spacecraft missions. Multi-shock blankets are described in comparison with early protective metallic "bumpers" and with a somewhat more recent invention called the "multi-shock shield." A multi-shock blanket is a standalone, self-contained shield system that includes several layers of ceramic (or equivalent) shields separated by a flexible foam material. The flexible foam can be any lightweight, outer-space-rated, resilient compressible material. The blanket can be compressed, if necessary, prior to launch to accommodate more payload volume and then be deployed in orbit to provide maximum protection. The blanket can be tailor-made in sections or patches to cover any critical exterior surface. Simple hook-and-pile or snap attachments can be used to secure the blanket on the outside of a spacecraft. The multi-shock blanket provides the high performance of the multi-shock shield, but without need for a cumbersome structure like that needed to support the multi-shock shield.

This work was done by Bruce D. Dvorak of The Boeing Company for **Johnson Space Center**. *To obtain a copy of the report, "Multi-Shock Blanket" and copies of companion documents "Hypervelocity Impact Shield" (U. S. Patent 5,067,388) and "Multi-Shock Shield Support Study," see TSP's [page 1].*

Title to this invention has been waived under the provisions of the National Aeronautics and Space Act {42 U.S.C. 2457(f)}, to The Boeing Company. Inquiries concerning licenses for its commercial development should be addressed to

The Boeing Company
ATTN: Bruce Dvorak
5301 Bolsa Avenue
M/C H020-F603
Huntington Beach, CA 92647

Refer to MSC-22989, volume and number of this NASA Tech Briefs issue, and the page number.

BLANK PAGE

Computer Programs

Mathematics and Information Sciences

 BLANK PAGE

Mathematics and Information Sciences

LabVIEW as Flight Software With VxWorks Operating System

A development effort under way at the time of reporting the information for this article is directed toward producing a version of the LabVIEW data-acquisition software that would be suitable for use as flight software that could be executed in the VxWorks real-time operating system. The approach taken in this effort is to utilize the graphical programming capability of the LabVIEW software system to reduce the time and cost of developing flight software and, more specifically, to make it possible for ground-based software to be transferred to and utilized in a flight environment without rewriting the software. Thus far, a prototype flight version of LabVIEW has been developed to run in a VxWorks real-time operating system on an embedded processor for precisely controlling the temperature of an isolated cryogenic platform. (The temperature-control system is undergoing development for use in a future low-temperature microgravitational facility.)

This program was written by Edmund Baroth, Hyung Cho, Martin Barmatz, Philip Yates, and Philip Withington of Caltech for **NASA's Jet Propulsion Laboratory**. *For further information, see TSP's [page 1].*

This software is available for commercial licensing. Please contact Don Hart of the California Institute of Technology at (818) 393-3425. Refer to NPO-21124.

MPP Port of PVM to a Beowulf Computer System

The latest version of the Parallel Virtual Machine (PVM) computer program, denoted PVM 3.4.3, incorporates a massively parallel processor (MPP) software port that enables a user working on a computer outside a Beowulf system (a cluster of personal computers that run the Linux operating system) to incorporate the Beowulf system, as though it were a single computer, into the larger parallel machine administered by PVM. One of the big advantages of PVM is its ability to easily tie together heterogeneous computing systems. However, up to now, there has been no way to spawn a PVM task from outside a Beowulf system onto one of the nodes of the cluster if the node lacks an externally visible Internet Protocol (IP) address. The Beowulf/Linux port of PVM 3.4.3, denoted BEOLIN, was incorporated to overcome this limitation. The user need only add the externally visible address of the cluster host (one of the computers in the cluster that acts as a "front end" for communication between outside computers and the computers in the cluster). Thereafter, the BEOLIN code automatically assigns tasks to individual nodes within the cluster while hiding the details of the cluster from the user.

This program was written by Paul Springer of Caltech for **NASA's Jet Propulsion Laboratory**. *For further information, see TSP's [page 1]. PVM 3.4.3 is available for download from http://www.epm.ornl.gov/pvm/.*

This software is available for commercial licensing. Please contact Don Hart of the California Institute of Technology at (818) 393-3425. Refer to NPO-21048.

Software for Iterative Optimization of Plans

The Iterative Plan Optimization computer program automatically optimizes plans with respect to preferences expressed by human planners. This program incorporates a generalization of commonly occurring plan-quality metrics to provide a language for expression of preferences. The program implements a technique of iterative optimization that is a generalization of a prior technique of iterative repair, in which conflicts are detected and addressed one at a time until either no conflicts exist or a user-defined time limit has been exceeded. During iterative optimization, low-scoring preferences are detected and addressed individually until the maximum score is attained or until a user-defined time limit has been exceeded. A preference is a quality metric for a plan variable and can be improved by modifying the plan in a manner similar to that of repairing it. Plan modifications can include moving, creating, and deleting activities. For each preference, a domain-independent improvement-expert subprogram automatically generates the subset of modifications that could potentially improve the preference score.

This program was written by Steve Chien, Barbara Engelhardt, and Gregg Rabideau of Caltech for **NASA's Jet Propulsion Laboratory**. *For further information, see TSP's [page 1].*

This software is available for commercial licensing. Please contact Don Hart of the California Institute of Technology at (818) 393-3425. Refer to NPO-20922.

Software for Planning an SAR Antarctic Mapping Mission

The AMM Automated Mission Planner computer program was developed to save time and money by automating much of the planning of the Second RADARSAT Antarctic Mapping Mission (AMM), which was scheduled to take place at the time of writing this article. The planning problem for this and other RADARSAT missions is to select several hundred synthetic-aperture-radar (SAR) swaths that satisfy scientific objectives, which include coverage of a specified ground area. The selection is subject to constraints associated with the choice of downlink opportunities and with RADARSAT operation. These constraints interact in complex ways that make it difficult to design schedules manually. The software takes a set of SAR swaths and automatically generates a locally optimal downlink schedule and identifies violations of operational constraints; in so doing, the software frees the mission planner to concentrate on selecting swaths that satisfy scientific objectives. Mission planning time has thus been reduced from years to weeks.

This program was written by Barbara Engelhardt, Steve Chien, Russell Knight, Benjamin Smith, Darren Mutz, Robert Sherwood, Gregg Rabideau, and John Crawford of Caltech for **NASA's Jet Propulsion Laboratory**. *For further information, see TSP's [page 1].*

This software is available for commercial licensing. Please contact Don Hart of the California Institute of Technology at (818) 393-3425. Refer to NPO-21092.

Mechanics

Hardware, Techniques, and Processes

Books and Reports

Carbon Nanotube Bimorph Actuators and Force Sensors

These devices would make possible novel microelectromechanical systems, possibly even microscopic robots.

NASA's Jet Propulsion Laboratory, Pasadena, California

A proposal has been made to develop bimorph actuators and force sensors based on carbon nanotubes. The proposed devices could make it possible to generate, sense, and control displacements and forces on a molecular scale, and could readily be integrated with conventional electronic circuits. These devices could also enable the development of a variety of novel microelectromechanical systems, including low power mechanical signal processors, nanoscale actuators and force sensors, and even microscopic robots.

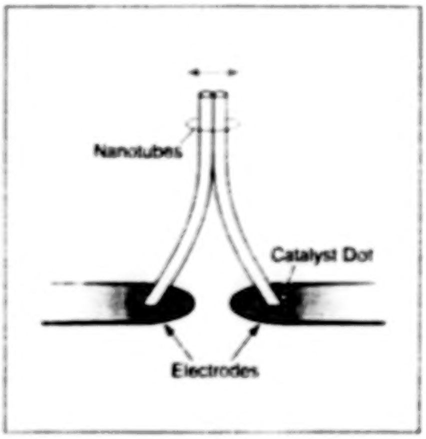

Carbon Nanotubes would grow out from catalytic metal dots on electrodes, eventually becoming attached to each other by van der Waals forces to form a bimorph actuator or sensor.

The proposed devices would exploit the dependence of nanotube length on charge injection that has been observed in mats of disordered carbon single-wall nanotubes (SWNTs) [Baughman, R.H., et al., "Carbon Nanotube Actuators," *Science* 284, 1340 (1999)]: the nanotubes become elongated or shortened when biased at negative or positive voltage, respectively. This result suggests that one could produce opposing changes in length in pairs of side-by-side, oppositely-biased nanotubes, resulting in a lateral deflection of the unsecured tube ends, as shown in the figure. Fabrication of such a nanotube bimorph device requires the ability to produce and join the tubes in the desired configuration with one end of each tube connected to a suitable electrical contact.

The proposed bimorph device could be fabricated by growing two nanotubes by chemical vapor deposition (CVD) on closely spaced catalyst dots over prepatterned bias electrodes on a substrate. It is likely that during the growth of the nanotubes, the van der Waals attraction would cause the nanotubes to become attached to each other along their sides, as shown in the figure. Because the electrical conductivity of a nanotube perpendicular to its length is much lower than the electrical conductivity along its length, this configuration should make it possible to maintain a significant differential voltage across the two nanotubes, as needed to cause a differential length change in the pair. Conversely, the application of a lateral external force to the tip of the pair should give rise to a voltage between the electrodes so that this device can also function as a sensitive force detector.

To be able to fabricate nanotube bimorph actuators with the configuration shown in the figure, it will be necessary to develop the means to control the positions and orientations of individual nanotubes on such substrates as silicon wafers. This is likely to entail the use of electron-beam lithography, lift-off, and etching for fabricating catalyst dots 5 to 15 nm wide on pre-patterned electrodes. Suitable catalyst materials could include Ni or alloys of Ni, Co, Fe, and/or Mo. In the contemplated CVD process, suitable precursor and carrier gases (e.g., methane, ethylene, or carbon monoxide plus hydrogen plus either argon or nitrogen) would interact with the substrate (which would be heated to a temperature between 600 and 950 °C), yielding selective growth of nanotubes out from the catalyst dots. There are numerous potential variations on this basic fabrication scheme, including orienting the dots so that the nanotubes grow parallel (instead of perpendicular) to the substrate surface and incorporating other materials to modify the electrical and mechanical properties of nanotube pairs.

This work was done by Brian Hunt, Flavio Noca, and Michael Hoenk of Caltech for **NASA's Jet Propulsion Laboratory**. *Further information is contained in a TSP [see page 1].*

In accordance with Public Law 96-517, the contractor has elected to retain title to this invention. Inquiries concerning rights for its commercial use should be addressed to

Technology Reporting Office
JPL
Mail Stop 249-103
4800 Oak Grove Drive
Pasadena, CA 91109
(818) 354-2240

Refer to NPO 21153, volume and number of this NASA Tech Briefs *issue, and the page number.*

Books and Reports

Airlocks for Pressurized Rovers

A report presents a survey of the design engineering and scientific literature on airlocks and on planetary-exploration vehicles ("rovers"), from the perspective of evaluating existing and potential design concepts for airlocks for pressurized rovers. The airlocks are the key to designing a pressurized rover that is useful and productive for the full range of activities and operational requirements. The challenge of the airlock problem for a pressurized rover arises from the perceived need for three different kinds of airlocks: one for ingress and egress for extravehicular activity (EVA) by astronauts, one for transferring samples for scientific study, and one for a habitat docking port. Each of these three airlocks has different design and operational requirements. Taking a design methodology focus, this review characterizes each prior pressurized rover design study as one of three alternative design approaches: Science-Driven, Mission-Architecture-Driven, or System-Analysis-Driven. The Science-Driven approach involved scientific exploration requirements as the main construct for rover design. The Mission-Architecture-Driven approach derives from a top-down design problem decomposition in which the mission architects and planners identify all the elements of the mission, the connections among them, commonality, and differentiation of parts and shared or unique capabilities. A System-Analysis-Driven approach to rover design embodies a bottom-up view of how all the parts of a particular product or vehicle must work together. The survey revealed that each of these design

approaches dictated, to a large extent, the type of airlocks that the prior studies considered. However, none of the surveyed studies included all three types of airlocks together in the conceptual design of a pressurized rover. The report surveyed airlock precedents for insight to future rover design. For sample airlocks, the report reviews the Spacelab, *Mir*, Columbus and the "Kibo" Japanese Experiment Module orbital laboratories. For docking pressure ports, the survey reviews the lessons of Skylab and Apollo-Soyuz, and considers the peculiar requirements of maneuvering a wheeled vehicle in a partial gravity field. For EVA egress and ingress, the report reviews from first principles comparative airlock concepts, including single volume, multiple volume and conformal, with attention to the problem of contamination control. The report presents a representative embodiment of each of these three airlock types through illustrations of a "simplified rover." The report concludes with a cogent set of design recommendations and characteristics for the three types of airlocks that would be particularly relevant to the design of a highly capable pressurized planetary rover.

This work was done by Marc M. Cohen of **Ames Research Center**. *To obtain a copy of the report, "Pressurized Rover Airlocks," see TSP's [page 1].*

ARC-14557

Machinery

Hardware, Techniques, and Processes

40 BLANK PAGE

Low-Power Shutter Mechanism for a Cryogenic Infrared Camera

The time-averaged power dissipation is <5 mW.

Goddard Space Flight Center, Greenbelt, Maryland

An assembly that includes electromechanical rotary actuators has been developed specifically for use as the shutter mechanism of a cryogenic infrared camera that will be part of an astronomical telescope. The camera will be cooled, by use of superfluid helium, to an operating temperature of 1.4 K. On command, the shutter mechanism rotates a mirror to one of two angular positions, denoted open or closed, at opposite ends of a 38° arc (see Figure 1). When the mirror is in the open position, light gathered by the telescope proceeds unobstructed to the focal plane of the camera; when the mirror is in the closed position, it obstructs the incoming light and provides a dark environment for calibration of the infrared photodetectors in the camera. The shutter mechanism is designed to be rugged,

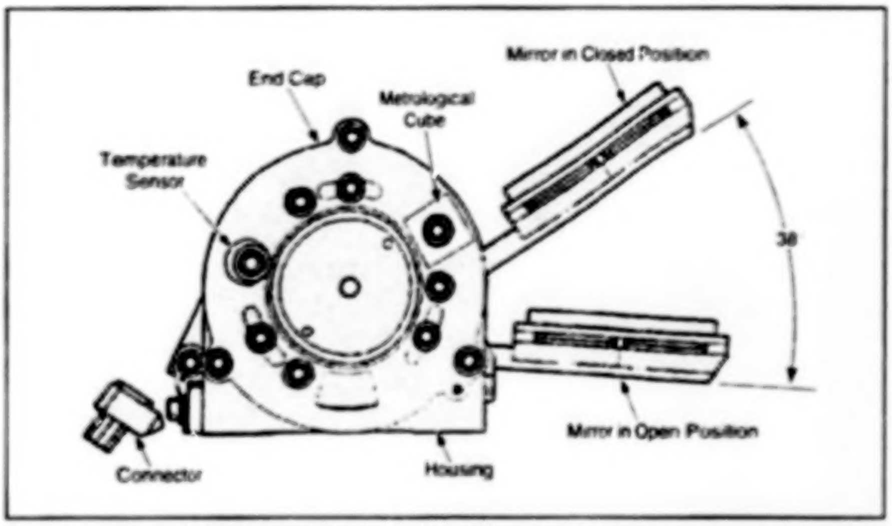

Figure 1. **A Mirror Is Positioned** at either end of a 38° arc by the shutter mechanism described in the text.

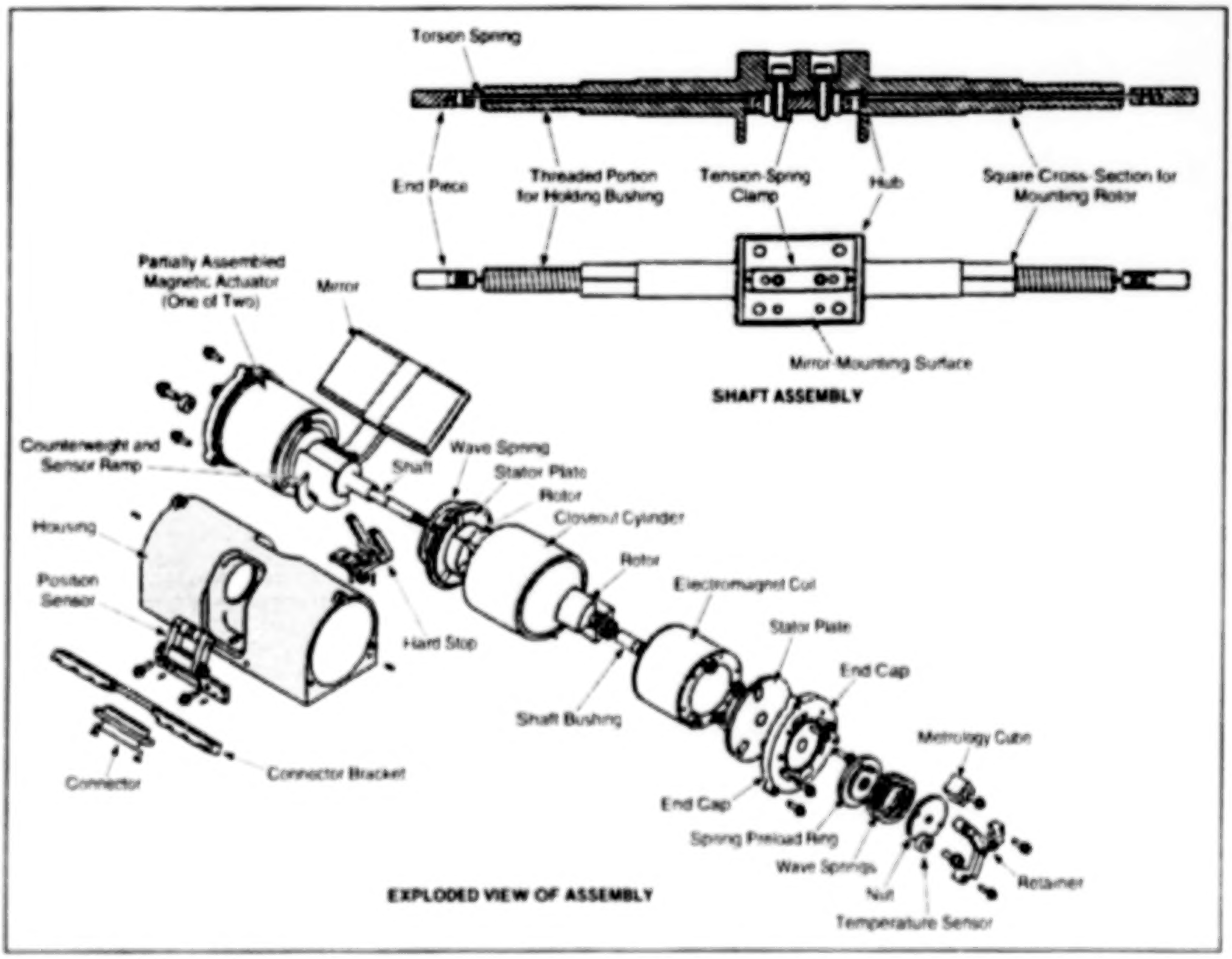

Figure 2. The **Shutter Mechanism** contains two variable-reluctance rotary electromagnetic actuators that oppose a torsion spring that biases the shutter toward the open position.

to have relatively low mass (≤1.6 kg), and to satisfy several requirements that pertain to mechanical and electrical performance in the cryogenic environment. A primary requirement is that the power dissipation averaged over time not exceed 5 mW.

Figure 2 depicts the components of the mechanism. The mirror is mounted on an arm that extends radially outward from an aluminum shaft. A tantalum counterweight mounted on the shaft opposite the mirror minimizes the offset of the center of gravity of the shaft, thereby minimizing moments that could be affected by gravitation, acceleration, and vibration. The shaft is supported by bushings that allow free rotation. The bushings fit into holes in end caps. The mating surfaces in the end caps are anodized and impregnated with poly(tetrafluoroethylene) to minimize friction. The shaft is machined to provide a central hollow that accommodates a beryllium copper wire, which serves as a torsion spring to bias the mirror in the open position.

The shaft supports two rotors that are magnetically soft and that are constrained in fixed angular positions relative to the shaft. These rotors are the moving parts of two variable-reluctance electromagnetic actuators. The stationary parts of each electromagnetic actuator include an electromagnet coil plus two magnetically soft stator plates and a magnetically soft close-out cylinder that completes the magnetic circuit. Electric current in the electromagnet coil of each actuator generates a magnetic field that is focused by the stators and passes through the rotor.

The geometry of the rotor and stators is such that the reluctance of the magnetic circuit varies with the angular position of the shaft, decreasing toward the closed position. As in any such actuator, this arrangement gives rise to a torque in the direction of decreasing reluctance. Hence, the application of current to the electromagnet coil gives rise to a torque that opposes the spring bias, turning the mirror toward the closed position.

A magnetic latch is essential for satisfying the requirement of low average power dissipation. The magnetic latch comprises a set of magnetically soft tabs that are affixed to the stators and extend from the stator faces. These tabs make contact with the rotors in the closed position. This contact effectively completes the magnetic circuit, reducing all airgaps to nearly zero, thereby effecting a large decrease in magnetic reluctance. In the low-reluctance condition, the mechanism can be held in the closed position, fighting the spring bias restoring torque with a lower current than is needed in the noncontact, higher-reluctance condition. The net result is that whereas a current of ≈55 mA is needed to close the shutter, a current of <1 mA is needed to hold it closed.

Of course, the naturally low electrical resistance of the electromagnet coil at the low operating temperature also helps to limit the power dissipation. A further reduction in power dissipation is obtained by use of an angular-position sensor and associated control circuitry: Inasmuch as the time taken in closing the shutter is about half a second, the control circuitry initially sends a high pull-in current pulse to the electromagnet, then quickly reduces the magnitude of the current to the holding level. The angular-position sensor informs the control circuitry when the mechanism reaches the closed position, making it possible to minimize the time spent at the higher pull-in current.

This work was done by David Scott Schwinger, Olaf Hakun, George Reinhardt, and Clarence S. Johnson of **Goddard Space Flight Center**. *Further information is contained in a TSP [see page 1].*
GSC-14341

Variable-Specific-Impulse Magnetoplasma Rocket

This rocket is expected to enable long-term human exploration of outer space.

Lyndon B. Johnson Space Center, Houston, Texas

Johnson Space Center has been leading the development of a high-power, electrothermal plasma rocket — the variable-specific-impulse magnetoplasma rocket (VASIMR) — that is capable of exhaust modulation at constant power. An electrodeless design enables the rocket to operate at power densities much greater than those of more conventional magnetoplasma or ion engines. An aspect of the engine design that affords a capability to achieve both high and variable specific impulse (I_{sp}) places the VASIMR far ahead of anything available today. Inasmuch as this rocket can utilize hydrogen as its propellant, it can be operated at relatively low cost.

The design of the VASIMR is so original that a prototype is being developed in collaboration with the Department of Energy and with the Oak Ridge National Laboratory and its Center for Manufacturing Technology. The VASIMR is expected to be commercially useful for boosting communication satellites and other Earth-orbiting spacecraft to higher orbits, retrieving and servicing spacecraft in high orbits around the Earth, and boosting high-payload robotic spacecraft on very fast missions to other planets. Similarly, the VASIMR should make it possible for robotic spacecraft to travel quickly to the outer reaches of the Solar system and begin probing interstellar space. By far, the greatest potential of the VASIMR is expected to lie in its ability to significantly reduce the trip times for human missions to Mars and beyond. This reduction in times is expected to enable long-term exploration of outer space by humans — something that conventional rocket designs now preclude.

Because the VASIMR uses plasma to produce thrust, it is related to several previously developed thrusters, namely, the ion engine, the stationary plasma thruster (SPT) (also known as the Hall thruster), and the magnetoplasmadynamic (MPD) thruster [also known as the Lorentz-force accelerator (LFA)]. However, the VASIMR differs considerably from these other thrusters in that it lacks electrodes (a lack that enables the VASIMR to operate at much greater power densities) and has an inherent capability to achieve high and variable I_{sp}. Both the ion engine and the SPT are electrostatic in nature and can only accelerate ions present in plasmas by means of either (1) externally applied electric fields (i.e., applied by an external grid as on an ion engine) or (2) axial charge nonuniformity as in the SPT. These ion-acceleration features, in turn, result in accelerated exhaust beams that must be neutralized by electron sources strategically located at the outlets before the exhaust streams leave the engines.

In the LFA, acceleration is not electrostatic but electromagnetic. A radial electric current flowing from a central cathode interacts with a self-generated azimuthal magnetic field to produce acceleration. Although LFAs can operate at power levels higher than those of either the ion engine or the SPT and do not require charge neutralization, their performances are still limited by

the erosion of their electrodes.

An MPD plasma injector includes a cathode in contact with the plasma. Although the plasma at the location of contact is relatively cold, the cathode becomes eroded and the plasma becomes contaminated with cathode material (typically tungsten). The erosion and contamination can contribute to premature failure and to increased loss of energy through radiation from the contaminants in the plasma. An equal limitation on performance is exerted by nonionized propellant in a high-power amplifier cavity that is part of the MPD; the reason for this limitation is that neutral atoms and molecules in this region lead to charge-exchange losses, which, in turn reduce the overall efficiency of the engine and increase the unwanted heat load on the first wall (the liner) of the MPD thruster.

The design of the VASIMR avoids the aforementioned limiting features. The VASIMR contains three major magnetic cells — the forward, central, and aft cells. A plasma is injected into these cells, then heated, then expanded in a magnetic nozzle. (The magnetic configuration is of a type known as an asymmetric mirror.) The forward cell handles the main injection of propellant gas and an ionization system; the central cell serves as an amplifier to further heat the plasma to desired magnetic-nozzle-input conditions; and the aft cell acts as a hybrid two-stage magnetic nozzle that converts the thermal energy of the fluid into directed flow while protecting the nozzle walls and allowing efficient detachment of the plasma from the magnetic field. During operation of the VASIMR, a neutral gas (typically, hydrogen) is injected into the forward cell, where it is ionized. The resulting plasma is then heated in the central cell, to the desired temperature and density, by use of radio-frequency excitation and ion cyclotron resonance. Once heated, the plasma is magnetically and gas-dynamically exhausted by the aft cell to provide modulated thrust. Contamination is virtually eliminated and premature failures of components are unlikely.

The VASIMR offers numerous advantages over the prior art:

- Its unique electrodeless design provides not only high thrust at maximum power but also highly efficient ion-cyclotron-resonance heating, and high efficiency of the VASIMR regarded as a helicon plasma source.
- Because the VASIMR operates at relatively high voltage and low current, its mass is relatively low. This means that a one-ship human mission will not depend on a high-energy, complex rendezvous near Earth to achieve escape velocity. Instead, a rapid interplanetary transfer will be achieved with an adaptable exhaust, which will provide optimal acceleration throughout the mission.
- The residual magnetic field of the engine and the hydrogen propellant will be effective as a shield against radiation.
- Because of its continuous acceleration, the VASIMR will be able to produce a small amount of artifical gravitation, thereby reducing the physiological deconditioning produced by weightlessness.
- The variability of thrust and I_{sp} at constant power will afford a wide range of capabilities to abort.
- Because hydrogen is the most abundant element in the universe, the supply of hydrogen could likely be regenerated *in situ*.
- The VASIMR is flexible and adaptable to both fast transfers of humans and slower high-payload robotic missions; hence, there would be no need to develop separate propulsion systems for missions of each type, and costs would be held down accordingly.
- Long-range benefits could be derived from the continued development of the VASIMR. The VASIMR can be expected to pave the way for fusion-driven plasma rockets. In addition, because the VASIMR is a high-I_{sp} rocket, the VASIMR concept can be expected to lead to lower initial mass in low Earth orbit, relative to nuclear, thermal, and/or chemical rockets.

This work was done by Franklin R. Chang Diaz of **Johnson Space Center**.

This invention is owned by NASA, and a patent application has been filed. Inquiries concerning nonexclusive or exclusive license for its commercial development should be addressed to the Patent Counsel, Johnson Space Center, (281) 483-0837. Refer to MSC-23041.

Magnetic/Extendible Boom Mechanism for Docking of Spacecraft

Docking loads can be smaller than those of prior mechanisms.

Lyndon B. Johnson Space Center, Houston, Texas

The magnetic/extendible boom docking aid is an improved mechanism that enables two spacecraft to capture and structurally mate with each other without inducing the large (and frequently excessive) loads encountered in docking by use of prior docking mechanisms. The capability afforded by this mechanism should prove invaluable when applied to the proposed International Space Station. This mechanism is relatively simple to construct, easily integrable into pre-existing docking hardware, and highly reliable.

The magnetic/extendible boom docking aid (see Figure 1) includes an assembly that contains a powered extendible boom with an electromagnet attached to the end; this assembly is mounted on one of two spacecraft that are to dock with each other. A target plate is affixed to the other spacecraft in the mating position. There can be as many points of contact and corresponding magnetic/extendible boom docking aids as are needed to effect safe and efficient docking. When the two spacecraft have moved into docking approach position, the booms are extended and the electromagnets are switched on. The spacecraft are made to approach each other very slowly until the electromagnets make contact with, and become magnetically attached to, the target plates (see Figure 2). The spacecraft are slowly drawn together by withdrawing the booms until docking mechanism latches are actuated. Mating is considered to have been achieved once the latches have been fully actuated.

Heretofore, two large spacecraft have been docked by causing the spacecraft to approach each other at a speed sufficient to activate capture latches — a procedure that results in large docking loads and is made more difficult because of the speed. The basic design and mode of operation of the magnetic/extendible boom eliminates the need to rely on speed of approach to activate capture latches, thereby making it possible to reduce approach speed and thus docking loads substantially.

Magnetic/extendible boom docking aids could be used on space station modules and on proposed lunar transfer spacecraft. They could also be used in the construction and operation of under-

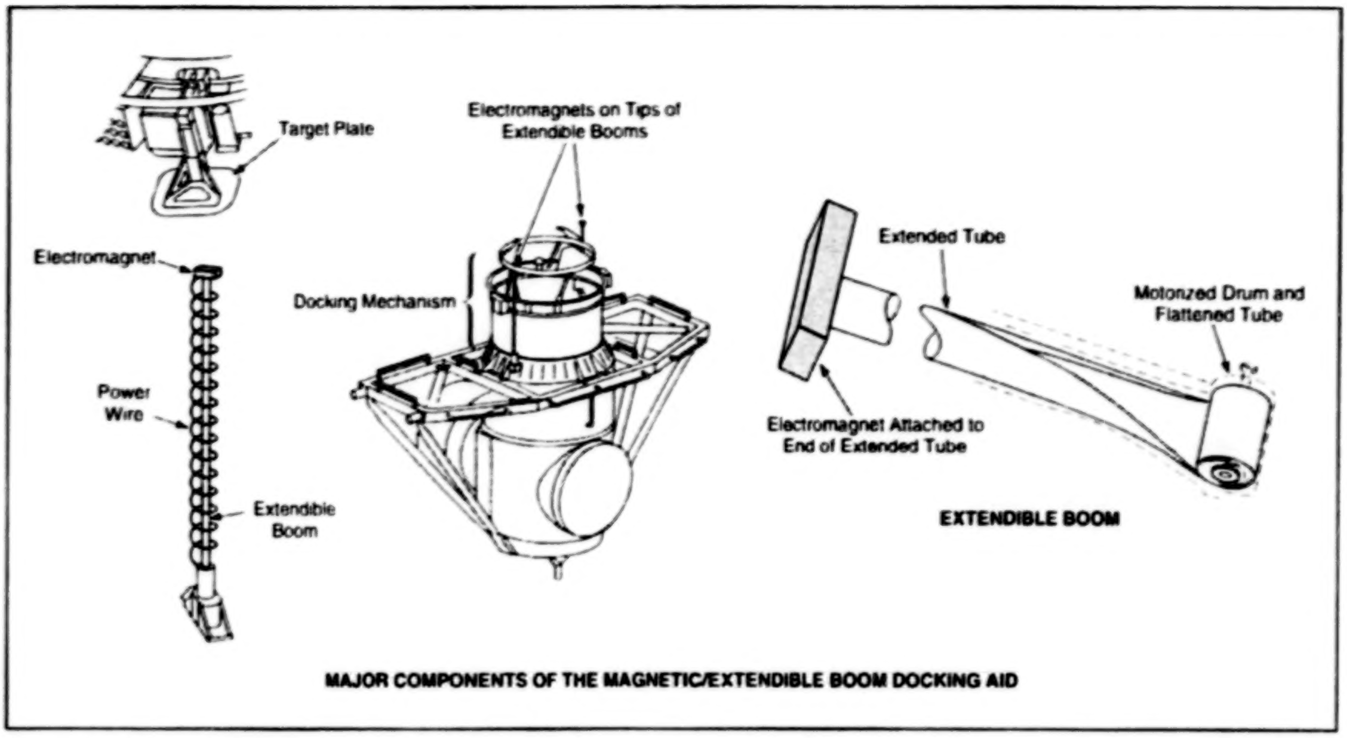

Figure 1. **The Boom Is Extended** by unrolling a flattened tube from a motorized drum. The boom is flexible in torsion and bending, stiff in tension, and back-driven in compression. The electromagnet on the tip of the boom attracts a target plate on the mating spacecraft.

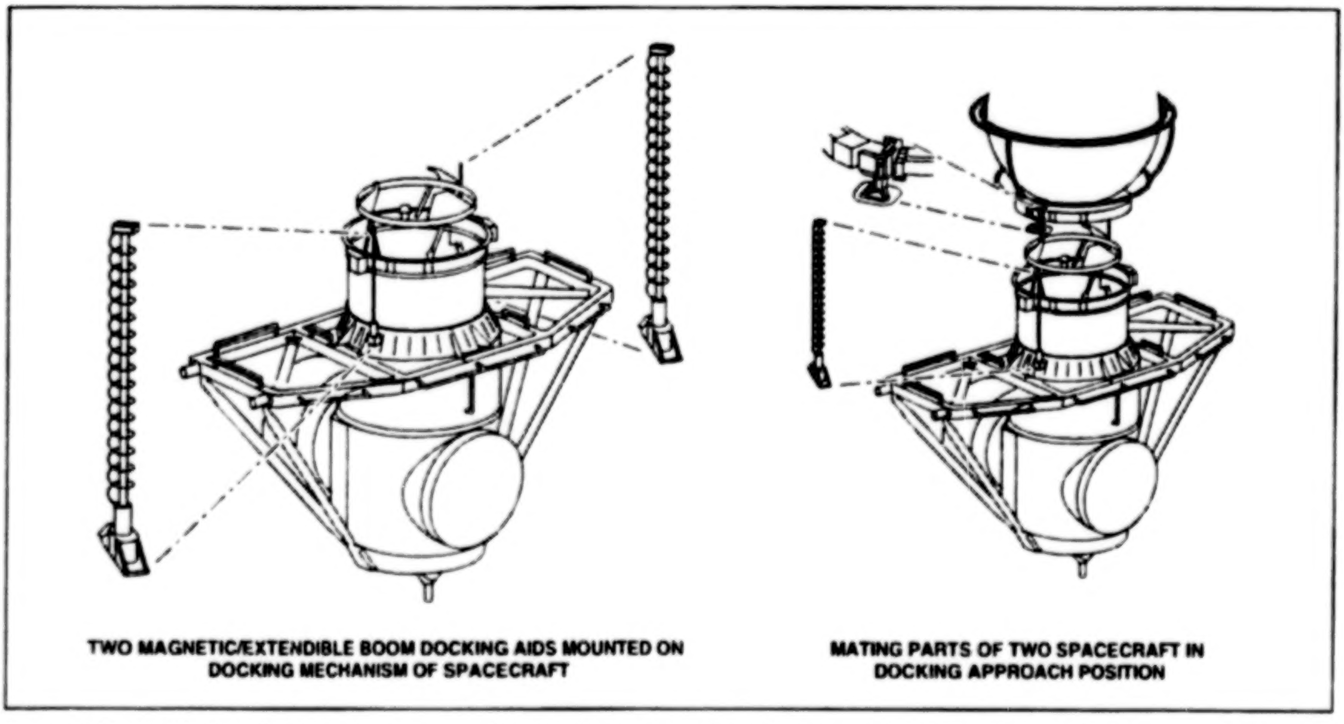

Figure 2. **Mating Parts of Two Spacecraft** approach each other very slowly until the electromagnets on the extendible booms of one spacecraft magnetically attract the target plates of the other spacecraft. Then the booms are retracted slowly to complete docking.

water habitat modules. Ultimately, they may even be useful in robotic operation of submersible vessels used to drill for oil. However, the commercial market may be limited because most land-based processes and equipment can withstand the high contact loads of conventional docking.

This work was done by William C. Schneider, Kornel Nagy, and John P. McManamen of **Johnson Space Center.** *MSC-22750*

Vapor-Compression Solar Refrigerator Without Batteries

Practical refrigeration is powered by an environmentally benign source.

Lyndon B. Johnson Space Center, Houston, Texas

A solar-powered vapor-compression refrigeration system developed for Johnson Space Center operates without batteries. The design of this system will make the cost of solar-powered refrigeration systems competitive and enable the use of such systems in long-distance spaceflights, military field operations, and other situations in which electric power for conventional refrigerators and freezers is unavailable.

The elimination of the need for batteries reduces (in comparison with a battery-powered system) the initial cost of the system and the cost of maintenance, as explained below. The system includes control circuitry that is connected directly to a solar photovoltaic (PV) panel and to a compressor. The system features a well-insulated cabinet, generous thermal-storage capability, and a high-efficiency cooling subsystem, that, together with the PV panel, make it possible for the cooled volume to stay cold year round. The technical feasibility and the potential economic advantage and environmental benefit of the system have been demonstrated in studies and in tests of a prototype of the system — a full-size, solar powered vapor-compression refrigerator in which the compressor is driven by a variable-speed, direct-current motor.

In a conventional refrigerator, a single-speed, alternating-current motor drives a vapor-compression cooling subsystem housed in a moderately insulated cabinet. Unfortunately, because a conventional refrigerator is designed to rely on an electric-power grid, its utility is restricted in spaceflight, military applications, or wherever electricity is unavailable or expensive. Prior solar-powered refrigerators included large batteries that were recharged by PV panels, or else thermal-cycle heat pumps rated at efficiencies lower than those of vapor-compression systems. Although the use of solar energy is environmentally benign, its widespread application has been slowed by a lack of cost-effective means. Where solar energy systems have been tried, they have lowered overhead, but because of the need for batteries and/or dc-to-ac power conversion, they have not eliminated it altogether. The present system eliminates the weights and costs of batteries and dc-to-ac power conversion subsystems.

The present system concept is flexible and allows variations of the basic design. The size of the cabinet can be chosen, with appropriate matching of the cooler, thermal-store, and PV capacities. In an alternative version of the system, one could reduce or eliminate thermal storage and incorporate electronic controls that would utilize backup power from a power grid or other source; this version could be cost-effective in an urban setting as well as in a remote setting. The scope of potential commercial applications could be widened by extending the concept to solar-powered freezers, ice makers, and air conditioners.

This work was done by Michael K. Ewert of **Johnson Space Center** *and David J. Bergeron III of Space Industries, a Division of GB Tech, Inc.*

This invention is owned by NASA, and a patent application has been filed. Inquiries concerning nonexclusive or exclusive license for its commercial development should be addressed to the Patent Counsel, Johnson Space Center, (281) 483-0837. Refer to MSC-22970.

Robot for Positioning Sensors in a Plant-Growth Chamber

The Advanced Life Support Automated Remote Manipulator (ALSARM) is a three-degree-of-freedom robotic system that positions an array of sensors inside a closed-system hydroponic chamber used in research on the production of biomass and the use of hydroponic subsystems of life-support systems. The array includes sensors to measure the light intensity, air temperature, infrared temperature, relative humidity, and airflow. The ALSARM operates under either automatic control by a personal computer or manual control through a teaching pendant (essentially, a hand-held box that contains switches and indicators wired to a plug for connection to the rest of the ALSARM control circuitry). The motivation for developing the ALSARM was the need to eliminate the leakage of the chamber atmosphere and the potential for contamination associated with the prior practice of opening the chamber so that technicians could enter to take environmental measurements. One especially notable feature of the ALSARM is a horizontal telescoping arm, through which power and signal cables for the sensors are routed. The cables are extended and retracted with the motion of the telescoping sections by use of a servomotor and gravitation, respectively.

This work was done by Michael D. Hogue, Andrew J. Bradley, Robert L. Morrison, and William C. Jones of **Kennedy Space Center** *and Roger W. Johnson, Ronald P. Enos, and Zhihua Qu of the University of Central Florida. Further information is contained in a TSP [see page 1].*
KSC-12084

4/6

BLANK PAGE

Fabrication Technology

Hardware, Techniques, and Processes

Venting Closed-Cell Foam Panels

Stresses cause by differential gas pressures are reduced.

Marshall Space Flight Center, Alabama

A technique for reducing in-flight loss of closed-cell foam insulation has been devised. In the original application, foam is used for thermal insulation on the external tank of the space shuttle. As the space shuttle ascends, aerodynamic effects cause an increase in surface temperature of the foam. This heating increases the internal cell gas pressure and reduces cell wall strength. The difference between the increasing pressure of the gases trapped in the foam cells and the decreasing pressure of the ambient air contribute to stresses that can break off pieces of foam during flight. Perforating the foam with small holes makes it possible for some trapped gases to escape, reducing the stresses sufficiently to keep the foam intact during ascent. This technique reduced in-flight foam loss by more than 95 percent. The vent holes could offer similar benefits in other applications where materials are subjected to thermal and pressure gradients.

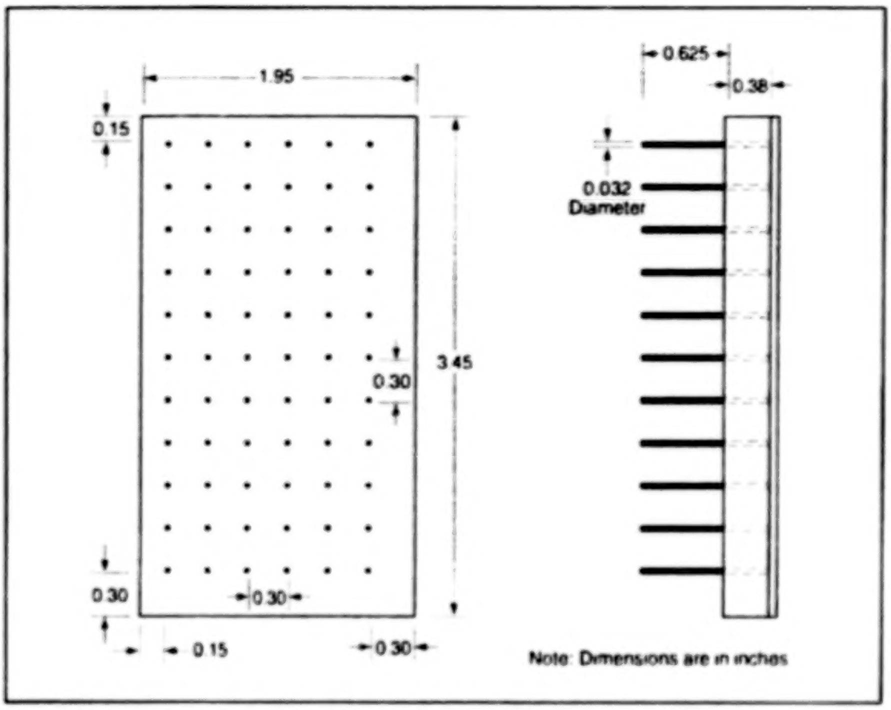

This **Tool Is Used To Perforate a Foam Panel** with holes in a square array.

A tool for making vent holes comprises a regular array (typically, a square pattern) of pins held in a backing plate. The shape of the array and the spacing, length, and diameter of the pins must be optimized for the particular material application, configuration, and environment(s). For the original space-shuttle application, the optimum dimensions were found to be those shown in the figure.

One needs at least two identical tools to ensure the regularity of the holes across a foam panel. To begin making the holes, one carefully places the first tool in the desired initial position with the pins in contact with the surface of the foam, then evenly and gently presses pins into the foam until the tips of the pins make contact with the substrate to which the foam is attached. The second tool is placed adjacent to the first tool, then pressed into the foam in the same way. Then the first tool is withdrawn and repositioned adjacent to (but on a different side of) the second tool, and so forth, until the pattern of holes extends over the desired panel area. The relative positions of the pins within each tool and the adjacency of the two tools ensure the proper positioning of the holes across the area.

This work was done by Hale Davidson of Lockheed Martin Corp. for **Marshall Space Flight Center.** *Further information is contained in a TSP [see page 1].*
MFS-31498

Thermal-Stress Technique for Cutting Thin Glass Sheets

Highly localized heating generates highly localized stresses.

Goddard Space Flight Center, Greenbelt, Maryland

A technique based on the generation of highly localized thermal stresses has been devised as a means of cutting both flat and curved glass sheets of thicknesses between 30 and 600 μm. The technique is reliable, accurate, and economical. The technique can be used, for example, to cut thin glass sheets for microscope slides and for covers on laptop-computer displays and other flat-panel displays.

Heretofore, thin glass sheets have been cut, variously, by use of lasers or by use of diamond tips and knives. Laser cutting is expensive. Diamond tips and knives generate microfractures that make glass sheets more susceptible to breakage along lines other than the intended cut lines. Cutting of thin, curved glass sheets by use of diamond tips and knives is expensive and difficult.

In the present technique, an electrically heated tungsten tip is applied to the glass to be cut. Because of the low thermal conductivity of glass, a large amount of heat can be concentrated in a narrow region surrounding the heated tip. The local concentration of heat gives rise to thermal stresses that can be large enough to break the glass locally and smoothly. As a result, from a macroscopic perspective, the heated tip works like a knife that cuts through the glass.

This work was done by William W. Zhang and Delmar H. Arbogast of **Goddard Space Flight Center.**
GSC-14364

50

BLANK PAGE

Mathematics and Information Sciences

Books and Reports

Books and Reports

Generating Commands for the Mars Polar Lander Robotic Arm

A report discusses the use of the Web Interface for Telescience (WITS) for visualization and command sequence generation in the Mars Polar Lander (MPL) mission. WITS, which has been described in prior articles in *NASA Tech Briefs*, is an Internet-based software system that enables geographically dispersed scientists and engineers to participate in sequence generation for planetary lander and rover missions. Public outreach versions of WITS enable the general public to use WITS to view mission images and plan and simulate their own missions. WITS enables scientists to view mission data and generate command sequences from their home institutions, making it unnecessary for them to travel to a mission control center to participate in the mission. The present report describes how WITS fits in the MPL mission operations architecture and how it was used for Robotic Arm and Robotic Arm Camera sequence generation.

This work was done by Paul Backes and Jeffrey Norris of Caltech and Kam Tso and Gregory Tharp of IA Tech, Inc., for **NASA's Jet Propulsion Laboratory**. *To obtain a copy of the report, "Sequence Generation System for the Mars Polar Lander Mission," see TSP's [page 1].*

In accordance with Public Law 96-517, the contractor has elected to retain title to this invention. Inquiries concerning rights for its commercial use should be addressed to

Technology Reporting Office
JPL
Mail Stop 249-103
4800 Oak Grove Drive
Pasadena, CA 91109
(818) 354-2240

Refer to NPO 20886, volume and number of this NASA Tech Briefs issue, and the page number.

Life Sciences

Hardware, Techniques, and Processes

Books and Reports

BLANK PAGE

Microwave-Sterilizable Access Port

Materials can be transferred into and out of closed bioreactors without contamination.

Lyndon B. Johnson Space Center, Houston, Texas

The microwave-sterilizable access port is an apparatus that functions in a simple, quick, and reliable manner to reduce significantly the risk of contamination during transfer of materials into or out of bioreactors or other microbially vulnerable closed systems. A major improvement over equipment developed previously for the same purpose, this apparatus can be expected to increase confidence in the microbial integrity of samples taken from closed systems. In tests, the original model of this apparatus exceeded expectations: Although it was rigorously challenged by a variety of microorganisms (e.g., *C. albicans, A. niger, S. faecalis, E. coli, K. terrigena, Ps. cepacia, B. pumilus, B. stearothermophilus*), it performed very well. The apparatus is easily adaptable to applications in cell culture and tissue engineering, and to applications in the production of diverse products that could include foods, drugs, bottled water, soft drinks, and fruit juices. By ensuring that sterilization can be achieved simply, reliably, and quickly, the microwave-sterilizable access port will facilitate collection of samples, delivery of nutrients, and harvesting of products, all without the potential for contamination of the experimental or production systems, samples, or the environment.

The microwave-sterilizable access port comprises two main assemblies: a microwave power source and an access port (see Figure 1). The access port includes a sterilization chamber, an in-line valve, and a specimen-transfer device. During normal operation, the in-line valve is closed and the bioreactor or other system of interest is isolated. The access port houses a cylindrical aperture into which the specimen-transfer device is inserted. At the bottom of the aperture is a smaller hole for access to the sterilization chamber. In preparation for sterilization and transfer of a specimen, a small amount (~500 μL) of distilled water is introduced into the sterilization chamber through the smaller hole, taking care not to deposit water within the larger cylindrical cavity. In further preparation for sterilization and transfer of a specimen, a specimen-transfer subassembly that comprises a pre-sterilized septum and the specimen-transfer device is inserted in the sterilization chamber, septum end first.

Positioning of the specimen-transfer device within the access port for insertion, sterilization, and puncture of the septum is controlled by a three-position rotating cam mechanism. Figure 2 shows the mechanism in the open, sterilization, and access positions. Rotation of the three-position cam to the sterilization position during insertion causes establishment of a septum seal, so that the chamber becomes closed to the outside. Once this seal has been established, electrical power is applied to a magnetron in the microwave-power source. Microwave power is coupled from the magnetron, via a coaxial cable, into the sterilization chamber, where the microwave power becomes further coupled to a silicon carbide block and with the small amount of water (microwaves

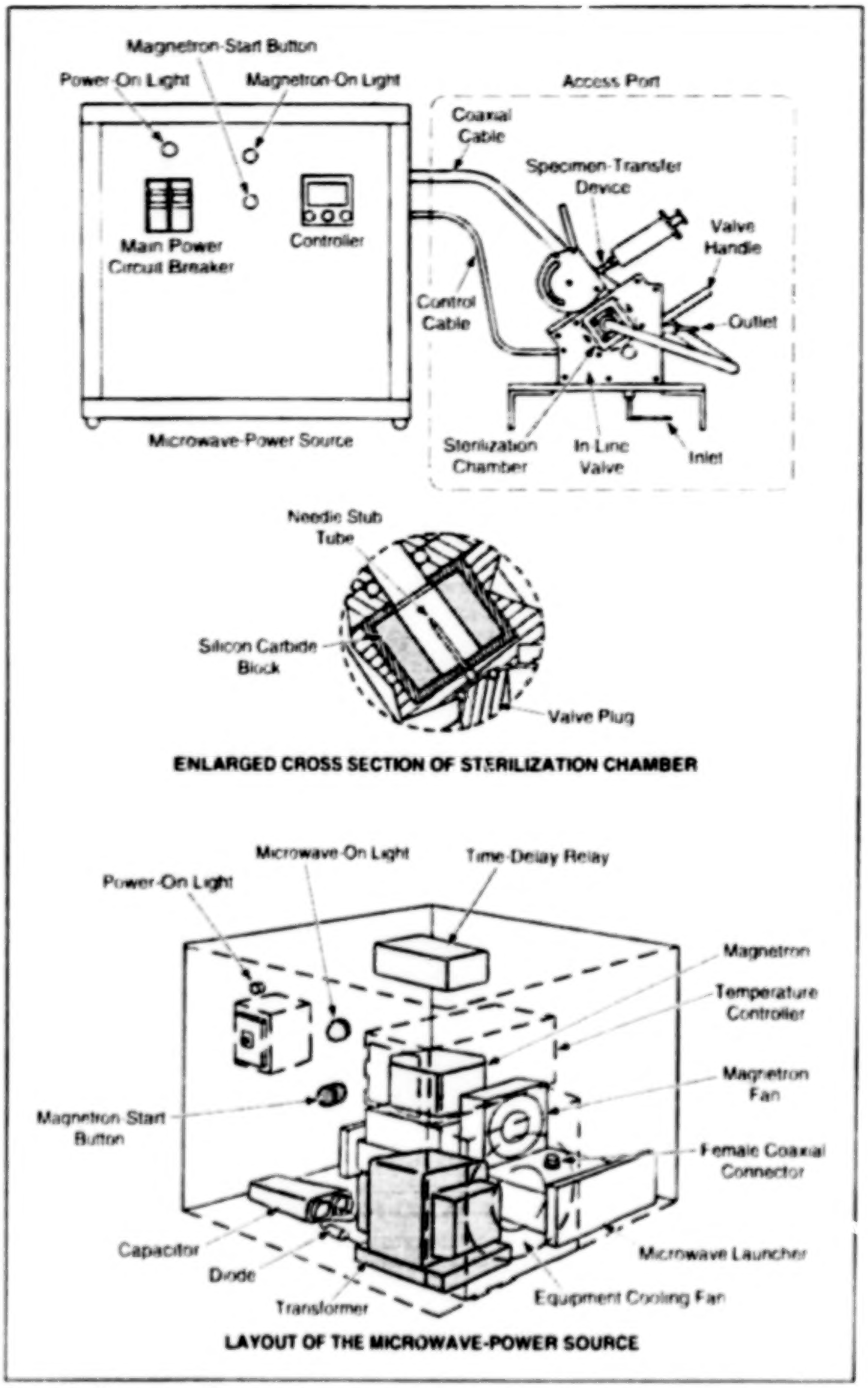

Figure 1. **Microwave Power** heats water to generate steam that sterilizes critical specimen-transfer components inside the sterilization chamber just before a transfer is effected.

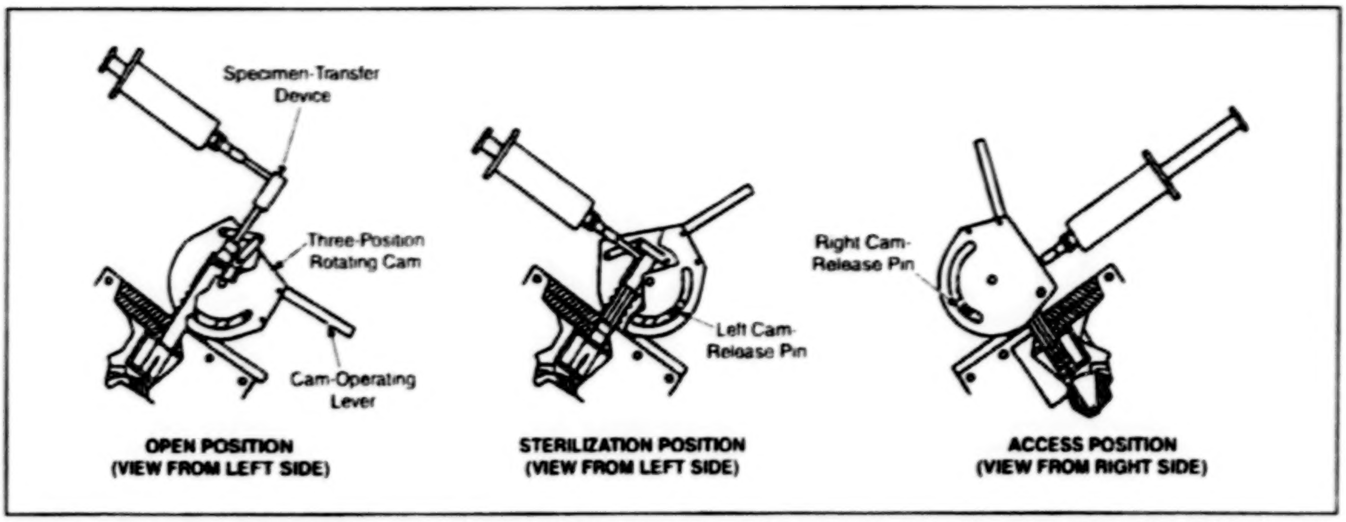

Figure 2. A **Mechanism That Includes a Three-Position Rotating Cam** positions the specimen during the various steps of the sterilization and specimen-transfer operations.

can couple strongly with lossy dielectric materials like H_2O and SiC) to produce heat. The heat causes the water to flash to superheated steam, which then pressurizes the chamber and sterilizes all exposed surfaces. The temperature is monitored with a thermocouple mounted in the SiC block.

When the temperature reaches ≈300 °C (≈572 °F) [typically after ≈30 seconds] the microwave power is automatically turned off and a solenoid vent valve opens, releasing a small amount of steam and condensate. The three-position cam is then rotated to the access position. During the rotation, the sterilized septum surface is pierced by a sterile needle stub tube that is part of the specimen-transfer device. Then access to the bioreactor or other closed system can be gained by turning the in-line valve to "access" position; once this has been done, a specimen can then be either collected from, or inserted in, the bioreactor or other system by use of a syringe that mates with the specimen-transfer device via a Luer lock connection. To terminate access to the system, the in line valve is closed, the three-position cam is returned to the open position, and the specimen-transfer device is removed.

A cabinet houses the magnetron, a microwave power controller, and other components of the microwave-power source. A time delay relay (TDR), which provides a fixed time safety limit, is set for ≈45 seconds and is latched "on" through the normally closed contacts of a temperature controller to enable sterilization to continue. Sterilization proceeds until the TDR is de-energized.

The totality of destruction of microbes was demonstrated in tests. More specifically, wet thermal sterilization of systems contaminated with a variety of bacteria, yeasts, and molds was demonstrated. It was also shown that by use of hydrogen peroxide solutions instead of pure water, equivalent sterilization levels could be attained at lower temperatures and shorter exposure times without producing the usual chemical contaminant residues. The utility of the microwave sterilizable access port was shown in repetitive transfers of sterile media through a sterilization chamber that was intentionally contaminated with 106 colony-forming units (CFU) of *B. stearothermophilus*, a thermophilic spore-forming bacterium used as the standard microbial challenge for wet-heat and steam-sterilization methodologies. Bidirectional transfer of sterile media was also demonstrated: at the end of the trial, no microbial survivors were recovered in any of 80 replicate experiments.

This work was done by Richard L. Sauer of **Johnson Space Center** *and James E. Atwater, Roger Dahl, Frank Garmon, Ted Lunsfort, William F. Michalek, and Richard R. Wheeler, Jr., of Umpqua Research Co.*

This invention is owned by NASA, and a patent application has been filed. Inquiries concerning nonexclusive or exclusive license for its commercial development should be addressed to the Patent Counsel, Johnson Space Center, (281) 483-0837. Refer to MSC-22802.

Treatment With Ferrates Eliminates DNA and Proteins

Water and perhaps air can be cleansed of microbiological (probably including viral) contamination.

NASA's Jet Propulsion Laboratory, Pasadena, California

Ferrate (VI) salts have been proposed for use in sterilizing water (perhaps also in sterilizing air). The iron in ferrate (VI) salts is in its highest oxidation state (VI), and these salts are extremely strong oxidants. In laboratory experiments, it was shown that treatment of DNA solutions with micromolar concentrations of potassium ferrate (VI) irreversibly inhibits further DNA polymerization and polymerase-chain-reaction (PCR) synthesis. Such treatment does not produce any toxic wastes; instead, what remains after treatment are iron ions, which can be recycled and which, in some applications, are useful as nutrients.

According to the proposal, ferrate (VI) derivatives fixed on various supports and carriers would be used to oxidize waterborne or airborne protein and deoxyribonucleic acid (DNA) molecules. Examples of suitable ferrate (VI) derivatives could include calcium ferrate, and barium ferrate, and inorganic polymers that carry ferrate (VI) ions. Further research is planned in order to develop materials, equipment, and procedures to implement these concepts.

This work was done by Alexandre Tsapin, Kenneth Nealson, and Michael Goldfeld of Caltech for **NASA's Jet Propulsion Laboratory**. *Further information is contained in a TSP [see page 1].*
NPO-20881

Books and Reports

Spacecraft-Facility Microbes Tolerate H_2O_2, NaCl, and Heat

A report describes experiments that were performed to isolate and characterize microbes that survive conditions of controlled circulation of air, desiccation, low nutrient concentrations, and moderately high temperatures in a spacecraft-assembly facility. These conditions are more severe than those to which the natural strains of the same microbial species are ordinarily exposed. This study is part of continuing research on related issues of (1) efficacy of sterilization (e.g., by use of H_2O_2 and/or heat) of spacecraft to be used in planetary exploration, (2) the use of selected microbes as indicators of the effectiveness of sterilization, and (3) the feasibility of commercial utilization of enzymes produced by microbes that tolerate severe conditions. Of the bacterial strains isolated (89 isolates) from the spacecraft-assembly facility, 44 percent exhibited intense growth at a temperature of 60 °C (thermophilic), and 50 percent did so in the presence of NaCl at concentrations as high as 10 percent (halophilic). In addition, 8 out of 24 thermophilic and halophilic strains also survived two or more cycles of exposure to vapor H_2O_2, which has come into wide use as a sterilizing agent in the pharmaceutical industry.

This work was done by Kasthuri Venkateswaran of Caltech for **NASA's Jet Propulsion Laboratory**. *To obtain a copy of the report, "Isolation and Characterization of Hydrogen Peroxide Resistant, Thermotolerant, and Halotolerant Microbes from a Spacecraft Assembly Facility," see TSP's [page 1].*

NPO-20980

END

12-4-01